1-1-1983

Structural testing of a three-story steel shear wall.

William Deforrest Bast

STRUCTURAL TESTING OF A THREE-STORY STEEL SHEAR WALL

by

WILLIAM DEFORREST BAST

A Thesis

Presented to the Graduate Committee

of Lehigh University

in Candidacy for the Degree of

Master of Science

in

Civil Engineering

Lehigh University

April 1983

This thesis is accepted and approved in partial fulfillment of the requirements for the degree of Master of Science in Civil Engineering.

May 9, 1983
Date

Professor Roger G. Slutter
Professor in Charge

Professor David A. VanHorn
Chairman, Department of Civil Engineering

ACKNOWLEDGMENT

This investigation was performed by the Operations Division of Fritz Engineering Laboratory at Lehigh University. Professor Lynn S. Beedle is the Director of Fritz Engineering Laboratory and Professor David A. VanHorn is the Chairman of the Civil Engineering Department. The testing program was sponsored by the United States Steel Corporation.

The author sincerely thanks his advisor, Professor Roger G. Slutter, for the guidance, help and patience that he has shown towards the author in both this specific testing program and the many others undertaken from the Summer of 1981 to the Spring of 1983. Professor George C. Driscoll and Professor Alexis Ostapenko also provided unsolicited words of advice and help which were greatly appreciated.

Testing could not have occurred without the expertise of Messrs. Robert Dales, Charles "Bud" Hittinger, Raymond Kromer, David Kurtz, Russell Longenbach, Hugh Sutherland, Kermit Eberts, Peter De Carlo, and Paul Kraihanzel. Their assistance in this particular test was outstanding and typical of their day-to-day performance. Messrs. William Frank and X. R. Wang assisted the author during testing. Mr. John Gera and Mrs. Sharon Balogh drafted the figures. A special word of thanks is given to Mrs. Dorothy Fielding for typing this manuscript in particular and her willingness to help those in need at Fritz Lab in general.

TABLE OF CONTENTS

TABLE OF CONTENTS (continued)

LIST OF TABLES

LIST OF FIGURES

LIST OF FIGURES (continued)

ABSTRACT

Limited theory and experimental test results exist concerning the behavior of stiffened steel panels with rectangular window cut-outs used as building shear walls. Due to these uncertainties, a test program was developed by a group of panel designers and was executed by the Fritz Engineering Laboratory at Lehigh University in December 1981.

The test program consisted of loading a three-story panel in compression along the diagonal to simulate shear loading. Measurements taken during testing included racking deformations and out-of-plane deflections in addition to strain readings at selected points on the specimen.

Test results indicate that analytical models can be used to predict the behavior of this type of structure within reasonable limits. Methods of predicting stresses, deformations, buckling and weld performance are outlined in this paper and compared to actual test values. The author provides interpretations of the test results and theory so that the behavior of steel shear walls may be better understood.

1. INTRODUCTION

The concept of providing stiffness for lateral loading in tall buildings through the use of steel shear walls is fairly new. In general, there are four ways to laterally stiffen buildings:

1. Moment resisting beam-to-column connections.
2. Diagonally braced frames.
3. Shear walls between columns.
4. Stiffened central core.

When shear walls are selected as the medium for providing added stiffness to a building, reinforced concrete walls are generally provided. The most recent development in the design of shear walls has been the selection of steel panels instead of reinforced concrete walls as the structural member used to provide lateral stiffness.

There are five advantages in selecting steel shear walls as opposed to reinforced concrete shear walls:

1. Decreased wall thickness.
2. Prevention of concrete construction pacing steel construction
3. Avoidance of complex concrete reinforcement.
4. Reduction in the total amount of steel needed in the structure (as much as 50%).

5. Reduction in the total weight of the structure. This in turn reduces the size of the seismic force that the structure will need to resist since the seismic force is directly proportional to the mass of the building.

These distinct advantages have caused structural designers to lean more towards steel panel shear walls within the last five years, as evidenced by the construction of the following buildings.[1,2]

1. Hyatt Regency Hotel (Dallas, 1978) - Stiffened steel shear walls (without window openings) were provided in the short direction of the structure and varied from a 13 mm (1/2 in.) thickness to a 29 mm (1-1/8 in.) thickness.

2. Los Angeles Olive View Hospital (Los Angeles, 1978) - The four-story structure contains both 16 mm (5/8 in.) and 19 mm (3/4 in.) thick steel plate shear walls.

3. H. C. Moffitt Hospital (San Francisco, 1978) - Steel shear walls were used to stiffen the 34 m (110 ft.) by 61 m (200 ft.) tower in the hospital structure.

As a further extension of the steel shear wall concept, the Welton Becket Associates, an architectural firm, devised a plan for the design of the Dravo Tower (Pittsburgh, PA.) for the United States Steel Corporation that incorporated structural steel shear walls as the architectural building facade. This meant that windows would need to be cut from the steel plate that would make the load bearing panel acceptable from an aesthetic viewpoint - a "first" in the design of steel shear walls.

The problem facing the project's structural engineers, Lev Zetlin Associates, was the unique problem of designing steel shear walls with window cut-outs that would adequately carry lateral wind loads with an appropriate safety factor and an acceptable amount of distortion.

2. BACKGROUND

A ten-step design procedure was developed by Lev Zetlin Associates for the design of the Dravo Tower panels and included the following items: [3]

1. Finite element analyses using plane stress elements.
2. Development of stress contour maps.
3. A computer program written to choose panel thickness' and stiffener locations.
4. Modeling an equivalent thickness panel to take into consideration the window openings.
5. Buckling analyses using the NASTRAN program.

Several approximations (e.g. the modeling of the panel-to-frame connections) were made in these analyses and some degree of uncertainty existed concerning the conservativeness of the approximations. The desire to confirm analytical results for strength, stiffness, and stability under shear loading of the designed panels led to the formation of a test program.

3. TEST PROGRAM

Lev Zetlin Associates devised a test program with the purpose of comparing actual results with analytical results obtained from theory relative to the strength, stiffness and stability of steel shear walls for the Dravo Tower.[4] The intent of the program was to use one typical panel design that could be specially fabricated for testing (and therefore could be loaded to failure) and perform a full-scale test on the specimen. Consequently, a test panel was selected from a group of varying size panels that had already been designed for the project.

The test panel selected was a three story stiffened plate structure measuring 11 m x 3 m x 6.35 mm (36 ft. x 10 ft. x 1/4 in.) fabricated entirely from ASTM A36 structural steel. Longitudinal and transverse stiffeners were welded to the interior side of the panel as shown in Figs. 1 and 2. Six windows, each measuring 2.14 m x 0.72 m (7 ft. x 2.4 ft.), were cut from the panel at United States Steel Corporation's fabrication shop. The plate was attached to a loading frame that consisted of W27 x 178 perimeter members with offset W14 x 90 spandrel beams at the ends and third points. Panel connections to the test frame existed primarily at the top, bottom and window areas of the panel and consisted of ASTM A490 high strength bolts as shown in Fig. 3. Additional panel connections were located above and below each window using channel sections that spanned the test frame columns.

The panel was to be loaded on its diagonal to simulate a racking or shear load that would be introduced to the panel along all four edges via the loading frame. For this purpose, two conditions were specified:

1. The loaded test frame corners had been bevelled and supplied with a bearing plate to provide the correct angle of loading at each corner as depicted in Fig. 4.
2. The test frame was to be laterally supported at each spandrel beam to prevent instability of the perimeter members.

In order to compare actual results with theory, the following measurements were required:

1. Out-of-plane deflections
2. Racking deflections.
3. Panel strains.
4. Stiffener strains.
5. Loading frame strains.

The methods of obtaining these measurements will be described in detail in Chapter 4.

In addition, the following changes or modifications were made to the test program by Fritz Engineering Laboratory in order to improve test result accuracy and to reduce the overall cost of testing:

1. One-half of the panel was completely instrumented, thereby taking advantage of symmetry of the structure.
2. Stiffening of certain sub-panel regions after buckling, a requirement in the original test program, was deleted.
3. The A490 bolts which connected the panel to the test frame were checked for proper preload to insure the behavior of friction-type connections.

4. TESTING

Prior to loading the test panel, several steps were required so that accurate measurements could be obtained.

First, electrical resistance strain gages were applied to both surfaces of the panel as shown in Figs. 5 and 6. Three-gage rectangular rosettes were used so that principal stresses could be readily computed. In addition, strain gages were placed on two stiffeners and at two locations on the test frame as shown in Fig. 7.

Second, the panel was "whitewashed" with a lime and water solution so that yielding of structural steel components during testing could be detected by eye by noting the locations of "flaking" of the whitewash. A grid was then created on the whitewashed surface using chalk lines shown in Fig. 8.

Third, three windows were fitted with rods on their diagonals, which were connected to Linear Variable Differential Transducers. This would allow the measurement of the changes in window diagonal lengths as detailed in Figs. 9 and 10.

Last, initial plate contours were established using the following procedure:

1. Initial column straightness and alignment were measured using an engineer's transit with the panel lying on its side.

2. A "ladder" of dial gages was then run across the face of the panel and supported on its ends by the frame columns as illustrated in Figs. 11 and 12. Grid point contours were measured to the nearest 0.025 mm (0.001 inches).

3. A computer program was written to establish relative contour values for the unloaded panel, taking into account loading frame column misalignment and warping in addition to initial out-of-plane deformations due to fabrication.

For the purpose of testing, the panel was lifted into the vertical position and placed in the compression loading space of Lehigh University's 22.25 MN (5,000,000 lb.) Baldwin hydraulic testing machine as exhibited in Figs. 13 and 14. The remaining requirements of the test program were subsequently executed and the panel was readied for testing.

Testing of the panel took place on December 10 and 11, 1981. On the first day of testing, the panel was successfully loaded to a vertical load of 2.45 MN (550 kips). At this load, lateral deformation of the panel was evident but disappeared as the load was reduced at the end of the day, exhibiting elastic behavior. During the second day of testing the panel was loaded to 3.34 MN (750 kips), at which time failure of welds occurred and the load on the panel dropped by approximately 668 kN (150 kips).

During the conduct of the test, measurements were taken at selected intervals in the following manner:

1. All strain gage and LVDT readings were printed by an electronic data acquisition system and simultaneously punched on paper tape.
2. Racking deflections of the panel edges and corners were measured using plumb bobs and adjustable-elevation lab tables as presented in Figs. 15 and 16.
3. Out-of-plane deformations were obtained by running a dial gage ladder across the whitewashed face of the panel starting at the bottom of the panel and progressing upwards to a level just above the second story windows.
4. Out-of-plane deformations of the loading frame were monitored using an engineer's transit.

Subsequent to the failure of welds, the panel was unloaded and testing was considered to have been completed.

5. SUMMARY OF TEST RESULTS

The ultimate vertical load of 3.34 MN (750 kips) that the panel withstood represented a design factor of safety of 3.33. In general, the panel behavior followed predicted values; the panel design itself can be viewed as being conservative.[5]

A computer program was written to reduce the strain gage readings for the panel rosette gages to principal stresses, maximum shear stress, and stresses relative to a coordinate axis established by the panel geometry (σ_x, σ_y and τ_{xy}). These values are tabulated in Appendix A.

In-plane deformations that were measured are described in Figs. 17 and 18 and tabulated in Appendices B and C.

Another computer program was written to reduce the measured out-of-plane contours to relative contour values considering the misalignment of the test frame columns and the initial out-of-plane contours due to fabrication. The program then utilized another computer program which was available on permanent file for plotting contour maps of the panel using the relative contour values. The initial panel contour map under no load is shown in Fig. 19. This map was developed from contour values obtained while the panel was lying on its side. Figure 20 shows the panel contours obtained due to a vertical "holding" load of 107 kN (24 kips). Panel contours

relative to the 107 kN load map are shown in Figs. 21 and 22 corresponding to vertical loads of 1.34 MN and 2.45 MN (300 kips and 550 kips), respectively.

In addition to the measurements taken above, the following significant results were obtained during testing:

1. At a vertical load of 1.11 MN (250 kips) the panel produced a loud noise similar to that produced by bolted plates undergoing an initial slip under load.
2. At a vertical load of 1.89 MN (425 kips) a slip of the long bolted joints connecting the panel to the test frame caused a noticeable drop in load.
3. At a load of 3.34 MN (750 kips) weld failures occurred. Upon closer examination of the unloaded panel, four longitudinal stiffeners sustained weld failure at the continuity weld connecting the longitudinal stiffener to the horizontal stiffener. The location of weld failures are indicated in Fig. 7 and shown in detail in Figs. 23 and 24.
4. The sub-panels that were predicted to undergo elastic buckling first experienced the greatest amount of out-of-plane deformation. These sub-panels are noted in Fig. 1, noticeable in Figs. 21 and 22, and shown in detail in Fig. 25.

Subsequent to unloading very slight permanent deformations remained in those panel areas that experienced the greatest out-of-plane deformation. This permanent set can be attributed to changes in the bolted joint forces and residual stress patterns rather than from gross yielding of the panel plate material.

Mechanical testing of the panel plate material revealed a yield strength of 296 MPa (42.9 ksi) as opposed to the nominal value of 248 MPa (36.0 ksi) required by ASTM A36.

6. THEORETICAL ANALYSES AND CONSIDERATIONS

Theoretical analysis of the test panel by the structural engineer, in conjunction with current steel and building design codes, prescribed a design shear load of 267 kN (60 kips) or a vertical testing machine load of 1001 kN (225 kips). The panel, when tested, exhibited a linear behavior to loads well in excess of the design load.

This section will present various analysis methods which were considered by the author for analyzing the complex structure of the panel. The validity and accuracy of these methods will be discussed in the next chapter.

6.1 Finite Element Method

The finite element method is clearly the best way to model and analyze a structure consisting of plates, stiffeners and rectangular holes. Many computer programs are currently available and economically feasible to use in performing an analysis of this type. As previously noted, the structural engineer for the Dravo Tower project made extensive use of FEM programs in designing the shear walls. However, repetitive and iterative uses of FEM programs in the preliminary design phase may become both cost prohibitive and inefficient. It is the intent of this report, therefore, to simply mention the possible use of FEM programs and their evident

success in analyses of this type; simpler and less expensive analysis techniques will instead be presented and discussed. The latter methods would be best-suited for arriving at a preliminary panel design which could then be refined, using finite element techniques for the final design.

6.2 Vierendeel Truss Analogy

The panel can be perceived as a modified Vierendeel truss, supported at its two unloaded corners by moment-free pins as shown in Fig. 26. A truss of this type requires moment-resisting connections and an involved analysis.[6] Before performing this type of analysis, however, two key factors must be considered:

1. What are the member sizes and properties to be used in the analysis and what are their effective sizes and properties?
2. How is the load transmitted from the building or test frame to the panel?

6.2.1 Effective Width Considerations

The effective width of a structural component can be defined as that portion of the component that can be considered in design for resisting the applied loads. The concept is illustrated in Fig. 27. Two methods can be used in determining effective widths:

1. Select member effective widths using a reference manual such as AISI's COLD-FORMED STEEL MANUAL, or

2. Develop effective widths from mathematical models.

The test panel possessed three stiffener sizes:

1. 102 mm x 13 mm (4 in. x 1/2 in.)
2. 127 mm x 13 mm (5 in. x 1/2 in.)
3. 152 mm x 10 mm (6 in. x 3/8 in.)

These stiffeners were intermittently welded to the panel plate as shown in Fig. 2. Using the panel geometry as a basis for determining various members of a Vierendeel truss, flat width-thickness ratios can be obtained from Fig. 26:

Member	w/t
Edge Columns	56
Center Column	136
Edge Beams	116
Center Beams	256

Using the COLD-FORMED STEEL MANUAL as a guide, the following equations yield effective b/t ratios:[7]

$$\text{For } w/t > \frac{171}{\sqrt{f}},\ \frac{b}{t} = \frac{253}{\sqrt{f}}\left[1 - \frac{55.3}{(w/t)\sqrt{f}}\right] \qquad (1)$$

and

$$\text{for } w/t > 60,\ \frac{b_e}{t} = \frac{b}{t} - 0.10\ [w/t - 60] \qquad (2)$$

Using f, the actual stress in the member, as approximately 152 MPa (22 ksi) and substituting the effective width, b_e, for each stiffener in each member is equal to 127 mm (5 inches). It is important to note that the effective width is the same for each stiffener regardless of the size of the stiffener.

The second method by which effective widths may be determined makes use of the Airy stress function which satisfies equilibrium and compatability equations for plane stress problems:[8]

$$\nabla^4 \phi = 0 \tag{3}$$

where

$$\frac{\partial^2 \phi}{\partial_x{}^2} = \sigma_y \tag{4}$$

$$\frac{\partial^2 \phi}{\partial_y{}^2} = \sigma_x \tag{5}$$

$$- \frac{\partial^2 \phi}{\partial_x \partial_y} = \tau_{xy} \tag{6}$$

Using several assumptions, the most significant being infinite stiffener spacing, an expression can be developed for the effective width:

$$b_e = \frac{2}{3 + \nu} \frac{\Sigma \frac{1}{\alpha_i} \frac{Nxy_i \sin \alpha_i x}{(3 - \nu)(1 + \nu) I_r + 4h/\alpha_i (S^2 + r^2)}}{\Sigma \frac{N_{xy_i} \sin \alpha_i x}{(3 - \nu)(1 + \nu) I_r + 4h/\alpha_i (S^2 + r^2)}} \tag{7}$$

N_{xy} is the uniform shear load applied to a member and must be approximated using a Fourier series approximation for use in this equation. Using a three non-zero term series expansion, effective widths can be determined at mid-length (s = L/2) for a given member:

Stiffener Size (mm)	b_e at x = L/2 (mm)
102 x 13	1245
127 x 13	1118
152 x 10	1092

The effective width for these members varies sinusoidally along the length; an average effective width can be determined by integration, realizing that the maximum b_e occurs at midlength (x = L/2):

Stiffener Size (mm)	Average b_e (mm)
102 x 13	787
127 x 13	711
152 x 10	686

Last, a reduction factor for b_e must be used to consider finite stiffener spacings. Use of reduction factors based on c/L ratios yields the following b_e's:[9]

Stiffener Size (mm)	b_e, mm (inches)
102 x 13	187 (7)
127 x 13	178 (7)
152 x 10	686 (27)

By comparison, the analytical method for determining b_e considers stiffener size and arrives at much larger effective width sizes than what would be used if other guidelines were incorporated. For this particular problem, the analytical method shows that full "member" sizes can be used in design and analysis in the Vierendeel truss model, whereas other guidelines suggest a reduction in member properties. The former method will be used, therefore, for the analysis of this problem because it does account for varying sizes of stiffeners.

6.2.2 Panel Loading

The idealized panel loading is that of a uniformly distributed shear load along the four edges of the rectangular structure. In actuality, however, a uniquely different loading system exists due to the presence of long bolted joints along the edges of the panel. Joint behavior can be predicted to a certain extent based on theory, but needs refinement for the problem at hand.

Up to the slip load of a bolted joint, a triangular stress distribution can be assumed to exist in the bolts and joint member due to strain variations through the joint.[10] After slip of the joint, a triangular stress distribution can again be assumed to exist in the components of the joint which is now in bearing. This stress distribution results in the "unbuttoning effect" at ultimate load which can be referenced in the literature. At this point it is important to realize that most slip load data and joint behavior is based on research which was concerned with typical structural

connections, i.e., bolt spacings of 76 to 102 mm (3 to 4 inches) and maximum joint length of 1.42 m (56 inches). For the test panel the six bolted connections that were located at the window openings were 1.42 m (56 inches) long and had bolt spacings of 102 and 203 mm (4 and 8 inches); the two connections at the top and bottom of the panel were 1.78 m (70 inches) long with bolt spacings of 127 and 254 mm (5 and 10 inches); see Fig. 3. Therefore it is hard to predict the structural joint behavior for this problem due to the lack of research in the area of very long bolted joints and large bolt spacings; however, two methods of predicting the load transfer from the test frame to the panel can be identified.

First, a uniform distribution of load can be assumed. This assumption is based on the notion that the panel is nearly completely attached to the test frame along all four edges and therefore receives a uniformly distributed shear loading from the frame.

Second, a type of triangular load distribution can be assumed. This assumption is based on the previously mentioned research and will more objectively be defined in the next chapter.

Both of the above assumptions will be used in the analysis of this problem in this paper. An attempt at precisely determining the manner and distribution of panel loading will be considered to be beyond the scope of this thesis.

6.3 Plane Stress Behavior

Another method for predicting panel stresses using plate theory is available through the use of the Airy stress function, Equations 3 through 6, which was previously used for effective width determination.[8] The two major pitfalls that occur as a result of applying this method to the problem at hand are: (1) inability to take the window openings into account, and (2) inability to consider the stiffness contribution of the stiffeners. This analysis, therefore, will merely consider a flat plate of uniform thickness loaded by a distributed shear load along all four edges. Also, the method of finite differences will be used to solve the differential equation in Eq. 3.

The variable $\emptyset$ in Eq. 3 can be obtained at desired points on the panel by using the method of finite differences in conjunction with the "Frame Analogy" as described in Ref. 8. Once $\emptyset$ is known, the stresses at the corresponding points can be computed by using the finite difference approximations in differential equations 4 through 6.

This method will be used in this report as a way of obtaining nominal stresses in those portions of the panel which are not affected by the assumptions made in the analysis; i.e. those portions of the panel that are a considerable distance away from window openings and stiffeners. For the purpose of the analysis, a grid spacing of 0.61 m (2 feet) will be used for solving for the unknown $\emptyset$ using the method of finite differences.

6.4 Window Deformation

Perhaps the most critical in-plane deformation associated with a load-bearing building facade is the window deformation. Several past incidents of problems with building windows cracking, falling out and not fitting properly can be attributed to lack of knowledge regarding window opening displacements. There are two methods by which the change in length of the window diagonals can be predicted.

First, the window can be assumed to be a flat steel plate loaded by a uniformly distributed shear load. This, of course, assumes that the window opening is sufficiently stiffened by the stiffeners that lie within 51 mm (2 inches) of its edges so that the opening actually behaves as a solid panel. With the original window diagonal measuring 2.15 m (84.55 inches), the corresponding change in length per 445 kN (100 kips) of vertical load would be 0.051 mm (0.002 inches).[11]

Second, the deformations of the entire panel associated with the Vierendeel truss analogy can be incorporated into the prediction of the change in length of window diagonals. By computing the diagonal change of the whole panel modeled as a Vierendeel truss, the same percentage change can be applied to the window openings. It will be shown in the next chapter that the corresponding change in diagonal lengths per 445 kN (100 kips) of load as predicted by this method yields values that are seven times greater than the values obtained in the first method.

It is expected that the second method would yield better predictions of panel window behavior since the assumption made in the first method has no substantiated theoretical basis. Therefore, the Vierendeel truss analogy will be used in this paper for predicting window diagonal deformations.

6.5 Buckling

The finite element analysis used by Lev Zetlin Associates predicted elastic buckling to begin at the two sub-panel regions shown in Fig. 1. Predicting the buckling of these same panels using other techniques can be accomplished using the following methods.

Reference 8 provides an equation for the determination of a critical shear stress for a rectangular plate:

$$\tau_{xy_{cr}} = \frac{\pi^2 E}{12(1-\nu^2)} \frac{1}{(b/h)^2} K_s \tag{8}$$

where

$$K_s = 5\left(1 + \frac{1}{\alpha^2}\right) \tag{9}$$

and

$$\alpha = \frac{a}{b} \tag{10}$$

For the two sub-panel sizes in question, each measuring 0.84 x 1.53 m (33 x 60 inches), $\tau_{xy_{cr}}$ equals 69.7 MPa (10.1 ksi).

Although the panel itself is subjected to a loading of pure shear, the sub-panels are subjected to a different type of loading primarily due to the presence of the window openings. Therefore the likely possibility of normal or direct stress must be considered.

Using equations similar to Eq. 8 but using a K value of 6.25 (representing the maximum buckling coefficient for simply supported edges), critical normal stress values of 20.3 MPa (2.94 ksi) and 67.1 MPa (9.73 ksi) can be obtained for the long and short directions, respectively, of the sub-panel plate region.

For the case of combined shear and direct stress, Ref. 12 provides an interaction formula which, when satisfied, indicates a critical stress combination:

$$R_s^2 + R_x = 1 \tag{11}$$

where

$$R_s = \tau/\tau_{cr} \tag{12}$$

and

$$R_x = \sigma/\sigma_{cr} \tag{13}$$

This report will use the stresses predicted by both the Vierendeel truss analogy and the plane stress method in conjunction with Eqs. 11 through 13 to predict the buckling condition for the subpanel regions in question.

6.6 Weld Behavior

Testing of the three-story shear wall was terminated when fracture of stiffener welds occurred. It is important, therefore, to be able to properly identify the strength and behavior of the panel's structural welds so that the overall panel performance will meet expectations. Research data is readily available and can be used to determine the behavior of the welded details in the test panel.

The integrity of the welds connecting the panel to the stiffeners and the latter to other intersecting stiffeners plays an important role in the panel's behavior. All the welds were designed as fillet welds and were apparently intended to develop the full strength of the connected parts. It is also important to note that, although the direction of loading of a welded detail is not a consideration in the design strength of the weld, significant behavioral differences exist between longitudinally and transversely loaded weld groups.

Reference 13 notes that the ultimate load of transversely loaded welded joints connected using E70 electrodes is 1-1/2 times that of longitudinally loaded joints, whereas the deformation at ultimate load of the latter is four times that of the former. These results are verified in Ref. 14 where tests on 6.4 mm (1/4 inch) E60 welds exhibited an ultimate load of 2.72 kN/mm (15.5 kips/inch) when loaded at a transverse angle of 90^{o}. This information can be used to verify the compatability of the weld design with the

joined members; it is of particular interest to examine the predicted behavior of the connection containing the intersection of a 152 mm (6 inch) horizontal stiffener with a 127 mm (5 inch) interrrupted vertical stiffener.

Knowing that the ultimate shear stress of a transverse fillet weld is 1-1/2 times that of longitudinal fillet welds or 0.8 - 1.3 times the nominal electrode tensile strength, the ultimate load for the 127 mm (5 inch) stiffener connection can be computed to be 498 to 712 kN (112 to 160 kips).[15] The corresponding ultimate load of the stiffener base metal material is a nominal load of 645 kN (145 kips). The weld design and component strength are compatible and the detail can be expected, therefore, to develop the full strength of the structure in question.

This is just one detail that can be evaluated and designed based on past research and existing codes. Other details for longitudinally loaded welds can be evaluated in a similar manner. The general behavior of the welds in the panel will be examined in the next chapter, where a comparison of theory to actual results will be presented and discussed.

7. COMPARISON OF THEORETICAL ANALYSES WITH EXPERIMENTAL RESULTS

The purpose of this chapter is to compare and discuss the correlation between theoretical analyses, as presented in Chapter 6, with experimental test results so that an understanding of the accuracy and applicability of theory can be better understood.

7.1 Vierendeel Truss Analogy and Plane Stress Behavior

An existing structural analysis computer program (utilizing the direct stiffness method) was used to obtain normal and shearing stresses at the strain gage locations. Full member sizes were used as indicated in Fig. 26 and cross-sectional properties were computed. A uniform shear load was applied to the structure to simulate loading frame conditions. The results of this analysis appear in Tables 1 through 11.

A computer program was written to solve for the unknown $\emptyset$ in the plane stress problem using finite differences. Again, a uniform shear loading was applied to the structure. Normal and shearing stresses at strain gage locations were then computed using Eqs. 4 through 6. The results of this analysis also appear in Tables 1 through 11.

A comparison of these two differing theories with experimental results can best be made by examining each individual stress location and discussing particular trends or observations that occur there. General conclusions can then be made by noting the accuracy of the correlations at each particular gage location.

Gages 1-3

Front-to-back correlation of actual panel stresses is not good and indicates out-of-plane bending at this gage location. The truss analogy yields normal stresses only in the x-direction (since a beam member was used) and gives values within 40% of the actual values. Shearing stress is best approximated by the plane stress analogy but is approximately 65% low at all load levels; much of this low value can be explained by the corresponding "missing" steel plate area due to the windows. Since the panel has 37% less area due to the window cutouts, the stresses predicted by the plane stress method should be amplified by the inverse of 0.63 or 1.59.

Since this gage is in a "solid plate" area that is a finite distance away from window openings and stiffeners, low normal stresses exist as predicted by the plane stress analogy. Shear stresses are 1.65 times that expected by this method. There is no effect due to slip of the bolted connections in the stress measurements at this location.

Gages 4-6

σ_y and τ_{xy} correlate well from front-to-back. The truss analogy yields values of σ_y that are 1.50 to 1.95 higher than actual; shear stress values are 20% lower than results. Normal stress in the x-direction is low as is required by the boundary conditions provided by the window.

In general, this location's stress field is best approximated by the truss analogy. The strain gage is next to a window and therefore only longitudinal stresses can be transferred due to lack of constraint in the x-direction. This gage does not show any joint-slip effects.

Gages 7-9

Normal and shearing stresses correlate well on both sides of the panel. The values of σ_y and τ_{xy} correlate within 15% and 10%, respectively, with actual test results. Transverse normal stresses are near zero as assumed in the truss analogy and as necessitated by the window effects.

Gages 10-12

Lack of correlation between front and back readings indicates out-of-plane bending at this gage. Average σ_x and σ_y results yield low stresses as predicted by the plane stress method. Shearing stresses as expected from the plane stress method are half of corresponding test results.

Overall, normal stresses at this location are closely approximated by the plane stress method; shearing stresses are amplified by a factor of 2.00 (gages 1-3 contained a factor of 1.65) due to the window cut-outs. This gage can also be considered to be located in a "solid plate" region.

Gages 13-15

This gage possessed readings that did not correlate well from one side to the other. Stress reversal from the first to second loading and, in particular, the shear stress on the back during the first loading between 1.78 and 2.23 MN indicate stress changes due to slip of a bolted joint. The truss analogy closely approximates σ_x and τ_{xy} up to the point of slip. The longitudinal stress, σ_y, reads near zero as it should since this gage is directly above a window.

Gages 16-18

Normal and shearing stresses are in very good agreement on both sides of the panel. The truss analogy predicts σ_y and τ_{xy} as 70% higher and 20% lower than results, respectively. This gage is also near a window and is best approximated by the Vierendeel truss analogy.

Gages 19-21

Out-of-plane bending is indicated by stress sign reversal from front-to-back. The horizontal normal stress, σ_x, is low as it should be at this gage location. However, the truss analogy yields compressive σ_y stresses whereas the gage reads tensile stresses. Shearing stresses are best approximated by the plane stress analogy but are 40-70% high.

This gage is difficult to approximate because: (1) it is located near the inflection point in the column (near the center of the window) and therefore low positive or negative stresses can be encountered within a short distance of the gage, and (2) the gage is within 19 mm of a welded stiffener.

Gages 22-24

Poor correlation of stresses from front-to-back indicates combined bending and direct stress. Stress reversal in the second day of loading indicates effects of joint slippage. The average normal stress values are low and correlate very well with the plane stress analogy; shear stresses as predicted by this method agree within 15-40%. This gage is in a solid plate region and is best approximated by the plane stress analogy.

Gages 25-27

Good correlation exists between the gages on the front and back sides of the panel. The transverse normal stresses (σ_x) are not low since the gage location is far enough from a window so that constraint is developed in this direction. The truss analogy approximates σ_y and τ_{xy} within 25%.

Gages 28-30

Bending of the panel prevents good correlation of gage results from one side to the other. Bolted joint slip effects are quite evident as indicated by stress reversals from loading one to loading two. The Vierendeel truss analogy agrees with actual test results within 10% up to the slip load. Longitudinal stresses are low as governed by the window boundary conditions. Shearing stress values are approximated best by the plane stress method but are still off the mark by 50-100%.

Gages 31-33

The front gage gives irrational results during both the first and second days of loading. Using the back gage as a reference, σ_y correlates with the truss analogy within 20%; σ_x develops due to constraint, and shearing stresses correlate best with the plane stress analogy (amplification factor = 1.43).

shear loading, a semi-triangular shaped loading was applied to the model using a shear distribution of 49%, 42% and 9% at the first, second and third floor levels, respectively. The results of this analysis do not yield better results overall. First floor gages experience greater stresses with this loading method than before and consequently better agree with test results. Second floor gages are also predicted to have higher stresses when in fact the test results show stresses that are not as high. Third floor level stresses are not dramatically changed.

The panel loading distribution is not uniform, and it is not as greatly concentrated at the two loading points as the column gages indicate; rather, the true load distribution can be expected to be somewhere between these extremes. Error in the readings of the column strain gages may occur due to bending of the column since strain gages were applied to only one side of the web. Further indications of load distributions are exhibited by the window diagonal deformations.

7.2 Window Deformation

Using the same structural analysis program that was used in the Vierendeel truss analogy, overall panel corner displacements were obtained as shown in Fig. 28. The panel diagonal measurement changed by 0.0166% due to the uniform shear loading applied. This same percentage of change, as applied to the window diagonals, yields a 0.356

mm (0.014 inches) change per 445 kN of vertical load. As previously noted, this value is seven times greater than the predicted value for a "steel plate window" under shear loading.

A table of test results and predicted measurements is presented in Tables 13 and 14. The two major diagonals of three windows were monitored and their respective length changes are shown in the table. Since the diagonal shortening and lengthening deformations should theoretically be equal, an average absolute deformation value is also tabulated to account for anti-symmetric distortion. The last column in the table represents the percentage of total window deformation for each particular window. Each window would receive 33-1/3% of the total window deformation under a uniformly distributed shear loading. This, however, does not occur due to the long bolted joints connecting the test frame to the panel.

The first loading results indicate that the third floor window received 25% of the total distortion, whereas the second and first floor windows received 55% and 49%, respectively, of the same phenomena. Since these numbers total 129%, it can be stated that a 29% error exists between predicted and actual measurements.

The second loading results indicate percentages of total deformation of 39%, 38% and 34% for the third, second and first floor windows, respectively. The percentage error between theoretical and experimental results is now reduced to 11%, and a much more even load distribution is apparent. The window deformation results, therefore, provide yet another indication of the load distribution on the steel shear wall.

7.3 Buckling and Out-of-Plane Deflections

In this section, a detailed discussion of the contour maps will be presented; subsequently, the use of the Vierendeel truss analogy combined with the plane stress analogy will be used to establish predicted instability conditions.

The contour map of the panel under no load shows initial out-of-plane deformations to be as great as 38 mm (1.5 inches) as shown in Fig. 19. This amount of eccentricity is tremendous when compared with the panel thickness of 6.4 mm. The various "hills and valleys" that are evident in this contour map help to explain the out-of-plane bending behavior noted at certain gage locations. The "steep" contours around the window openings are to be ignored in this figure because they result from the impossibility to obtain dial gage readings inside the perimeter of each window.

The 107 kN contour map, illustrated in Fig. 20, shows virtually the same general contour pattern as the unloaded panel contour - as it should. The exact amounts of out-of-plane distortion in these two contour maps do not check because the maximum and minimum peak contour levels occur at the top of the panel; these readings were not obtainable for the 107 kN map because the panel was in the standing position and its top story was inaccessible.

The 1.34 MN contour map shows values relative to the 107 kN map. Out-of-plane distortions were not measured at either loading above the second floor and therefore appear blank on this map. It

is of particular interest to note the development of buckling in the sub-panel region between the first and second floors. Out-of-plane deformations at this location equalled 1.52 mm at a load of 1.34 MN. The shape of the buckled sub-panel is noticeably rectangular in form and outlines the pattern of the panel stiffeners.

The 2.45 MN contour map also shows distortions relative to the 107 kN map. Several of the smaller magnitude out-of-plane distortions disappeared or remained the same size in going from a load of 1.34 to 2.45 MN, but the sub-panel region distortion between windows increased five-fold as the load increased 83%, measuring 7.62 mm at the first day's maximum loading condition. Again, the sub-panel bulging is shown to be confined fairly well to the area defined by the stiffeners.

Figures 29 and 30 show load versus lateral deformation plots for two grid points in the critical sub-panel region. Both grid points show ultimate buckling loads occurring at loads between 2.00 MN and 2.23 MN under initial loading conditions. However, the phenomena observed in these figures of linear second day loading up to 3.12 MN requires explanation.

There are three phenomena which can possibly explain the graphs shown in Figs. 29 and 30: (1) buckling of a structural component possessing initial out-of-straightness or load eccentricity, (2) residual stress effects, and (3) behavioral effects due to slip of the bolted joints.

When a structural member possesses initial imperfections and is loaded in compression, the phenomenon of bifurcation will not occur. Rather, nearly linear lateral deformation will occur up to an ultimate load - a load which is somewhat smaller in magnitude than the theoretical bifurcation load.[16] The two figures under examination exhibit this type of behavior on the first day of loading. The second day's loading behavior, however, is difficult to explain using this theory. There is no reason to believe that those initial out-of-plane flaws and load eccentricities that caused an ultimate load to be observed on the first loading would disappear and allow a higher ultimate load upon undergoing a second loading. This theory, therefore, explains the observed ultimate load of 2.00 to 2.23 MN, but fails to explain the complete hysteresis.

Residual stresses cause "early" yielding of structural steel components and usually possess values near the base material's yield stress in welded structures. Initial loading effects due to residual stresses yield non-linear behavior of the loaded member due to gradual yielding of the member cross-section; this effect is observed in the first day's loading. Upon unloading the structure and repeating the loading process, linear behavior should be observed up to the maximum load obtained on the first loading; then, non-linear behavior will again occur. This predicted behavior, based on knowledge of residual stress effects, does not occur during the second loading -- linear behavior exists beyond the first day's maximum load of 2.45 MN and continues up to an ultimate load of

3.34 MN. Residual stress effects, therefore, do not fully explain the figures in question.

Slip of the bolted joints under load causes stress reversal upon unloading. This statement is confirmed by several strain gages as previously noted. Loading the structure a second time will result in a shift of the initial "zero stress" level. The phenomenon is also evident in the strain gage readings and seems to occur between the loads of 890 and 1335 kN (200 and 300 kips). This means that the panel returns to its initial unloaded stress field at loads of 890 to 1335 kN and proceeds to behave as before upon further loading. The maximum load of 2.45 MN (550 kips) achieved on the first day of loading would thereby be equivalent to a load of 3.34 to 3.79 MN (750 to 850 kips) for the second day's loading.

It can be concluded that initial out-of-plane deformations and load eccentricities preclude the phenomenon of bifurcation from occurring and that residual stresses cause non-linear effects on the first loading of the panel. Non-linearity is erased during the second loading and an ultimate load is achieved which is considerably elevated due to stress reversals caused by slip of the bolted joints. Therefore, the ultimate panel load can be considered to be approximately 2.45 MN (550 kips).

Predicting the ultimate load of the panel can be accomplished by interpolating the results from the Vierendeel truss analogy and the plane stress method. These methods predict the following stresses at a load of 2.45 MN:

	Vierendeel Truss	Plane Stress
σ_x (MPa)	- 121.1	0.0
σ_y (MPa)	0.0	0.0
τ_{xy} (MPa)	68.7	33.0

Note that the Vierendeel truss stresses apply to panel locations near the windows and that the plane stress method is applicable to plate regions that are far removed from the windows and stiffeners. Therefore, by interpolating or averaging these results over the sub-panel region in consideration,

$$\sigma_{x\ ave.} = -60.6 \text{ MPa } (8.8 \text{ ksi})$$

and

$$\tau_{xy\ ave.} = 50.9 \text{ MPa } (7.4 \text{ ksi}).$$

Use of Eqs. 11 through 13 yields a value of 1.44 for the right side of Eq. 11, representing a 44% error in comparison to the actual ultimate loading condition. This method indicates a lower instability load and would thus be conservative in view of the experimental results.

7.4 Weld Behavior

One of the two stiffeners that were strain-gaged provides information that can be used to identify the strength of the welds at stiffener intersections. The strain gage locations are shown in Fig. 7; test results are tabulated in Table 15.

The test results show that the stiffener carried a tensile load of approximately 196 kN (44.1 kips) prior to failure of the weld connecting the 127 mm (5 inch) longitudinal stiffener to the 152 mm (6 inch) transverse stiffener. This load is, at best, only 39% of the predicted ultimate load for this connection. Three other similar welds were found to have failed in the same manner. The failure of these welds, which were loaded at an angle of 90° to the weld length, prompts several comments.

Close examination of the joint shown in Figs. 23 and 24 reveals the presence of welds from two different processes. Welds on one side of the joint were made using the manual shielded arc-welding process, while the other welds in the joint appeared to have been made using a semi-automatic continuous wire feed process. The differing processes yielded two different results: (1) the heat input and consequently the fusion created by the processes are considerably different, and (2) the weld leg sizes resulting from the processes also differed. The manual stick-welding process yielded inferior results in both cases: lack of fusion is evident in the manual welds, and the legs in these welds ranged from 4.8 - 8.1 mm (0.19 - 0.32 inches) compared with the design weld leg dimension of 6.4 mm (0.25 inch). The weld theoretically should fail in the throat; failure of a short-legged weld along the fusion line indicates faulty fabrication and consequently causes premature failure.

Welds loaded in a transverse manner exhibit greater strength and less ductility, as previously explained. Slight weld defects such as porosity, fit-up gaps and inclusions drastically reduce the strength of this type of weld. Gaps between welded components of up to 25% of the weld leg sizes are noticeable in Fig. 24 and further reduce the strength of the welds.

Finally, the failure of four longitudinal continuity welds prompts the question: "Why not provide continuous longitudinal stiffeners and interrupt the continuity of the shorter transverse stiffeners"? Although this question seems to point to the solution of the given problem, it may in fact simply shift the problem from the welds of the longitudinal stiffeners to those of the transverse stiffeners. Considerable normal stresses in both the panel plate material and stiffeners occur in both directions near the window openings, depending upon the location of the point in question. Since equal stiffener loads are expected and shown to exist in both vertical and horizontal stiffeners, the question of stiffener continuity priority is not pertinent; the quality of the designed welds is the controlling factor for the development of panel integrity.

8. SUMMARY AND CONCLUSIONS

It can be concluded that the design factor of safety for the tested steel shear wall equals 2.44. This number reflects the ultimate panel load achieved on the first day of loading and also the ultimate load achieved on the second day of loading, taking into account the shift in the "zero stress" level caused by slip of the bolted joints.

The analytical models used in this paper are accurate within 50% of actual test values. The Vierendeel truss analogy used the concept of shear lag and effective widths to obtain predicted stresses along the window perimeters. The effective widths used in this analysis were larger than those that would be selected from a reference handbook because of the relatively large cross-sectional stiffener sizes used in the panel design. An amplification factor of 1.59 used in conjunction with the plane stress analogy accurately predicts stresses for the remainder of the panel plate regions. This amplification factor is solely based upon the missing plate areas due to the presence of windows.

It has been shown that, although the actual shear distribution on the panel edges lies somewhere between a uniform and triangular distribution, the assumption of uniform shear loading yields acceptable stress results. A method of forecasting window

deformations has been presented and is accurate within 30%. Actual window deformation results show that a uniform shear loading can also be assumed in the analysis of panel in-plane deformations.

A method of predicting sub-panel elastic buckling was presented and yielded conservative results that were accurate within 44%. Panel contour maps showed large initial eccentricities due to fabrication which precluded the phenomenon of bifurcation from occurring. The maps also showed the confinement of the buckled zones to the sub-panel areas as defined by the stiffener grid pattern.

Finally, the weld failures that caused the failure of the panel were investigated. Differing weld processes and minor flaws combined to reduce weld strength by as much as 61%. The question of directional stiffener continuity was subverted and the quality of the welds was instead emphasized.

TABLE 1 RESULTS VERSUS ANALYSIS - GAGES 1-3 AND 34-36

Day	Load	RESULTS						ANALYSIS					
		FRONT			BACK			VIERENDEEL TRUSS			PLANE STRESS		
	(kN)	σ_x (MPa)	σ_y (MPa)	τ_{xy} (MPa)	σ_x (MPa)	σ_y (MPa)	τ_{xy} (MPa)	σ_x (MPa)	σ_y (MPa)	τ_{xy} (MPa)	σ_x (MPa)	σ_y (MPa)	τ_{xy} (MPa)
1	445	- 2.2	- 6.1	12.6	0.8	- 5.5	13.4	- 1.6	--	7.0	13.7	7.0	9.1
	890	- 5.8	-12.3	28.4	0.5	-12.3	30.6	- 3.2	--	14.0	27.4	14.0	18.2
	1335	- 5.5	-13.7	44.9	- 0.9	-18.9	47.4	- 4.8	--	21.0	41.1	21.0	27.3
	1780	16.4	66.4	33.9	- 3.2	-25.2	65.0	- 6.4	--	28.0	54.8	28.0	36.4
	2225	2.9	16.0	69.0	- 5.8	-32.0	82.1	- 8.0	--	35.0	68.5	35.0	45.4
2	445	0.2	26.8	11.2	- 7.7	- 3.8	18.6	- 1.6	--	7.0	13.7	7.0	9.1
	890	- 0.6	21.3	27.0	- 7.2	-11.1	35.2	- 3.2	--	14.0	27.4	14.0	18.2
	1335	- 1.5	16.6	42.0	- 6.6	-17.9	50.7	- 4.8	--	21.0	41.1	21.0	27.3
	1780	- 1.7	12.4	57.8	- 6.4	-25.5	66.9	- 6.4	--	28.0	54.8	28.0	36.4
	2225	- 1.8	8.3	74.5	- 7.9	-34.1	83.5	- 8.0	--	35.0	68.5	35.0	45.5
	2670	- 0.3	9.2	91.1	-11.4	-43.3	100.7	- 9.6	--	42.0	82.2	42.0	54.6
	3115	5.2	- 4.6	117.3	-30.4	-68.1	118.7	-11.2	--	49.0	95.9	49.0	63.7

TABLE 2 RESULTS VERSUS ANALYSIS - GAGES 4-6 AND 37-39

		RESULTS						ANALYSIS					
		FRONT			BACK						PLANE STRESS		
Day	Load (kN)	σ_x (MPa)	σ_y (MPa)	τ_{xy} (MPa)	σ_x (MPa)	σ_y (MPa)	τ_{xy} (MPa)	σ_x (MPa)	σ_y (MPa)	τ_{xy} (MPa)	σ_x (MPa)	σ_y (MPa)	τ_{xy} (MPa)
1	445	- 0.6	-10.4	10.4	0.8	- 9.9	10.8	--	- 18.5	9.7	2.8	3.8	7.3
	890	0.0	-22.8	21.4	0.2	-22.7	24.7	--	- 37.0	19.4	5.6	7.6	14.6
	1335	1.6	-34.1	34.7	0.4	-34.4	38.0	--	- 55.5	29.1	8.4	11.4	21.9
	1780	4.4	-49.4	44.1	- 1.5	-51.1	50.8	--	- 74.0	38.8	11.2	15.2	29.2
	2225	8.3	-60.4	71.8	- 3.0	-63.8	64.5	--	- 92.5	48.5	14.0	19.0	36.5
2	445	3.3	- 8.3	12.4	0.6	- 9.2	12.8	--	- 18.5	9.7	2.8	3.8	7.3
	890	3.7	-22.3	25.3	0.3	-23.3	26.4	--	- 37.0	19.4	5.6	7.6	14.6
	1335	5.0	-35.1	37.6	- 0.7	-36.8	39.5	--	- 55.5	29.1	8.4	11.4	21.9
	1780	6.7	-48.1	50.3	- 2.0	-50.7	52.9	--	- 74.0	38.8	11.2	15.2	29.2
	2225	9.5	-60.7	63.1	- 4.1	-64.8	66.3	--	- 92.5	48.5	14.0	19.0	36.5
	2670	13.6	-71.1	75.9	- 7.3	-77.3	80.0	--	-111.0	58.2	16.8	22.8	43.8
	3115	21.9	-72.5	88.3	-14.7	-83.5	34.6	--	-129.5	67.9	19.6	26.6	51.1

TABLE 3 RESULTS VERSUS ANALYSIS - GAGES 7-9 AND 40-42

		RESULTS						ANALYSIS					
		FRONT			BACK			VIERENDEEL TRUSS			PLANE STRESS		
Day	Load (kN)	σ_x (MPa)	σ_y (MPa)	τ_{xy} (MPa)	σ_x (MPa)	σ_y (MPa)	τ_{xy} (MPa)	σ_x (MPa)	σ_y (MPa)	τ_{xy} (MPa)	σ_x (MPa)	σ_y (MPa)	τ_{xy} (MPa)
1	445	- 2.7	- 25.7	9.9	0.3	- 24.6	7.9	--	- 23.7	9.7	- 1.6	1.9	5.7
	890	- 4.8	- 53.8	20.6	1.1	- 54.3	17.7	--	- 47.4	19.4	- 3.2	3.8	11.4
	1335	-527.2	-238.7	214.6	2.2	- 83.5	27.0	--	- 71.1	29.1	- 4.8	5.7	17.1
	1780	- 14.7	-115.9	47.3	6.0	-113.2	34.2	--	- 94.8	38.8	- 6.4	7.6	22.8
	2225	- 13.7	-143.5	61.5	8.1	-141.5	43.5	--	-118.5	48.5	- 8.0	9.5	28.5
2	445	- 6.1	- 20.8	12.5	2.2	- 23.8	9.2	--	- 23.7	9.7	- 1.6	1.9	5.7
	890	- 6.6	- 52.3	24.4	3.5	- 54.4	18.3	--	- 47.4	19.4	- 3.2	3.8	11.4
	1335	- 10.1	- 82.8	36.8	4.9	- 83.5	27.3	--	- 71.1	29.1	- 4.8	5.7	17.1
	1780	- 13.7	-113.2	49.7	6.3	-113.2	36.1	--	- 94.8	38.8	- 6.4	7.6	22.8
	2225	- 23.2	-145.6	65.2	7.9	-142.8	44.5	--	-118.5	48.5	- 8.0	9.5	28.5
	2670	-22.1	-169.7	77.3	9.7	-168.4	53.4	--	-142.2	58.2	- 9.6	11.4	34.2
	3115	-27.9	-188.4	102.1	12.6	-193.2	70.4	--	-165.9	67.9	-11.2	13.3	39.9

TABLE 4 RESULTS VERSUS ANALYSIS - GAGES 10-12 AND 43-45

		RESULTS						ANALYSIS					
		FRONT			BACK			TRUSS			PLANE STRESS		
Day	Load (kN)	σ_x (MPa)	σ_y (MPa)	τ_{xy} (MPa)	σ_x (MPa)	σ_y (MPa)	τ_{xy} (MPa)	σ_x (MPa)	σ_y (MPa)	τ_{xy} (MPa)	σ_x (MPa)	σ_y (MPa)	τ_{xy} (MPa)
1	445	- 3.6	- 9.2	8.7	6.1	- 1.1	17.0	3.0	--	10.0	- 0.1	0.0	6.0
	890	- 6.5	-18.1	18.7	12.6	- 4.1	38.8	6.2	--	20.0	- 0.2	0.0	12.9
	1335	- 5.8	-22.0	28.0	16.0	- 9.5	61.3	9.3	--	30.0	- 0.3	0.0	18.0
	1780	- 3.2	-22.3	35.8	15.1	-17.2	81.4	12.4	--	40.0	- 0.4	0.0	24.0
	2225	9.0	-12.8	40.0	4.5	-32.0	103.5	15.5	--	50.0	- 0.5	0.0	30.0
2	445	- 5.7	0.4	4.8	2.2	4.0	23.0	3.1	--	10.0	- 0.1	0.0	6.0
	890	- 6.0	- 7.0	15.0	7.5	- 1.3	43.1	6.2	--	20.0	- 0.2	0.0	12.0
	1335	- 4.6	-11.9	24.0	10.4	- 8.3	62.5	9.3	--	30.0	- 0.3	0.0	18.0
	1780	0.9	-13.0	31.9	8.8	-19.1	83.5	12.4	--	40.0	- 0.4	0.0	24.0
	2225	12.2	- 8.3	37.5	0.7	-33.5	104.2	15.5	--	50.0	- 0.5	0.0	30.0
	2670	29.9	4.6	40.4	-15.6	-52.1	123.5	18.6	--	60.0	- 0.6	0.0	36.0
	3115	26.0	- 0.3	36.2	-21.1	-47.5	133.2	21.7	--	70.0	- 0.7	0.0	42.0

TABLE 5 RESULTS VERSUS ANALYSIS - GAGES 13-15 AND 46-48

		RESULTS						ANALYSIS					
		FRONT			BACK			VIERENDEEL TRUSS			PLANE STRESS		
Day	Load (kN)	σ_x (MPa)	σ_y (MPa)	τ_{xy} (MPa)	σ_x (MPa)	σ_y (MPa)	τ_{xy} (MPa)	σ_x (MPa)	σ_y (MPa)	τ_{xy} (MPa)	σ_x (MPa)	σ_y (MPa)	τ_{xy} (MPa)
1	445	27.0	2.9	7.9	19.3	0.6	6.1	28.2	--	10.0	- 0.3	0.1	6.1
	890	61.3	6.2	19.9	44.4	1.1	14.6	56.4	--	20.0	- 0.6	0.2	12.2
	1335	95.9	10.8	32.2	67.5	2.0	23.9	84.6	--	30.0	- 0.9	0.3	18.3
	1780	122.1	12.1	40.4	81.4	-1.9	3.9	112.8	--	40.0	- 1.2	0.4	24.4
	2225	144.2	16.2	43.1	91.8	0.0	-57.5	141.0	--	50.0	- 1.5	0.5	30.5
2	445	1.0	- 5.5	- 3.4	- 4.8	1.9	-39.5	28.2	--	10.0	- 0.3	0.1	6.1
	890	35.4	- 1.4	7.1	19.2	2.4	-31.6	56.4	--	20.0	- 0.6	0.2	12.2
	1335	68.7	3.4	18.0	42.1	2.3	-24.7	84.6	--	30.0	- 0.9	0.3	18.3
	1780	102.8	8.6	29.6	64.9	1.7	-18.8	112.8	--	40.0	- 1.2	0.4	24.4
	2225	135.9	14.6	40.6	84.9	- 0.3	-14.6	141.0	--	50.0	- 1.5	0.5	30.5
	2670	160.0	18.0	46.8	98.0	- 1.2	-20.1	169.2	--	60.0	- 1.8	0.6	36.6
	3115	120.0	40.0	27.0	55.1	14.4	11.2	197.4	--	70.0	- 2.1	0.7	42.7

TABLE 6 RESULTS VERSUS ANALYSIS - GAGES 16-18 AND 49-51

		RESULTS						ANALYSIS					
		FRONT			BACK			VIERENDEEL TRUSS			PLANE STRESS		
Day	Load (kN)	σ_x (MPa)	σ_y (MPa)	τ_{xy} (MPa)	σ_x (MPa)	σ_y (MPa)	τ_{xy} (MPa)	σ_x (MPa)	σ_y (MPa)	τ_{xy} (MPa)	σ_x (MPa)	σ_y (MPa)	τ_{xy} (MPa)
1	445	- 1.7	-12.5	10.2	- 0.1	-12.0	10.9	--	- 23.3	10.1	0.0	0.0	6.1
	890	- 3.1	-27.7	22.4	1.0	-27.0	24.5	--	- 46.6	20.2	0.0	0.0	12.2
	1335	- 3.3	-42.0	35.6	1.7	-41.3	38.4	--	- 69.9	30.3	0.0	0.0	18.3
	1780	- 2.8	-56.1	49.3	1.5	-56.2	53.1	--	- 93.2	40.4	0.0	0.0	24.4
	2225	- 0.7	-67.3	62.7	0.8	-67.9	66.9	--	-116.5	50.5	0.0	0.0	30.5
2	445	2.6	- 6.5	11.7	- 3.6	- 8.6	14.9	--	- 23.3	10.1	0.0	0.0	6.1
	890	1.2	-22.8	24.6	- 2.9	-24.3	28.8	--	- 46.6	20.2	0.0	0.0	12.2
	1335	0.5	-37.7	37.1	- 2.4	-39.0	41.9	--	- 69.9	30.3	0.0	0.0	18.3
	1780	- 0.2	-53.1	50.0	- 1.5	-53.5	55.1	--	- 93.2	40.4	0.0	0.0	24.4
	2225	- 0.4	-67.6	63.1	- 1.6	-68.2	68.8	--	-116.5	50.5	0.0	0.0	30.5
	2670	0.7	-79.4	75.9	- 3.4	-78.7	82.8	--	-139.8	60.6	0.0	0.0	36.6
	3115	- 5.8	-78.7	92.5	- 5.6	-53.8	98.7	--	-163.1	70.7	0.0	0.0	42.7

TABLE 7 RESULTS VERSUS ANALYSIS - GAGES 19-21 AND 52-54

		RESULTS						ANALYSIS					
		FRONT			BACK			VIERENDEEL TRUSS			PLANE STRESS		
Day	Load (kN)	σ_x (MPa)	σ_y (MPa)	τ_{xy} (MPa)	σ_x (MPa)	σ_y (MPa)	τ_{xy} (MPa)	σ_x (MPa)	σ_y (MPa)	τ_{xy} (MPa)	σ_x (MPa)	σ_y (MPa)	τ_{xy} (MPa)
1	445	- 1.2	- 3.5	1.1	1.7	7.7	4.3	--	- 9.5	10.1	0.1	0.1	6.1
	890	- 3.8	- 7.7	2.9	5.3	19.8	9.5	--	-19.0	20.2	0.2	0.2	12.2
	1335	- 5.6	-11.2	4.7	7.2	32.4	15.3	--	-28.5	30.3	0.3	0.3	18.3
	1780	- 7.2	-13.5	6.2	9.1	46.2	22.1	--	-38.0	40.4	0.4	0.4	24.4
	2225	-10.2	-15.5	7.2	11.7	60.2	27.8	--	-47.5	50.5	0.5	0.5	30.5
2	445	- 6.8	- 1.2	3.1	5.1	14.8	8.8	--	- 9.5	10.1	0.1	0.1	6.1
	890	- 8.6	- 5.3	4.5	7.2	25.6	14.3	--	-19.0	20.2	0.2	0.2	12.2
	1335	-10.1	- 8.8	6.1	8.8	36.4	19.3	--	-28.5	30.3	0.3	0.3	18.3
	1780	-11.4	-12.6	6.9	10.4	48.2	24.4	--	-38.0	40.4	0.4	0.4	24.4
	2225	-13.2	-15.5	8.7	11.5	61.0	29.4	--	-47.5	50.5	0.5	0.5	30.5
	2670	-15.4	-16.8	10.1	12.3	73.1	35.3	--	-57.0	60.6	0.6	0.6	36.6
	3115	-14.1	- 8.6	8.8	- 3.3	58.7	62.0	--	-66.5	70.7	0.7	0.7	42.7

TABLE 8 RESULTS VERSUS ANALYSIS - GAGES 22-24 AND 55-57

		RESULTS						ANALYSIS					
		FRONT			BACK			VIERENDEEL TRUSS			PLANE STRESS		
Day	Load (kN)	σ_x (MPa)	σ_y (MPa)	τ_{xy} (MPa)	σ_x (MPa)	σ_y (MPa)	τ_{xy} (MPa)	σ_x (MPa)	σ_y (MPa)	τ_{xy} (MPa)	σ_x (MPa)	σ_y (MPa)	τ_{xy} (MPa)
1	445	- 1.5	1.8	7.7	0.1	- 3.1	-24.5	--	- 9.0	1.5	0.0	0.1	6.1
	890	- 2.7	4.2	17.3	1.5	- 5.3	-58.5	--	-18.0	3.0	0.0	0.2	12.2
	1335	- 3.3	7.5	27.5	1.2	- 7.1	-62.1	--	-27.0	4.5	0.0	0.3	18.3
	1780	- 1.8	10.6	38.2	2.2	- 7.8	-69.7	--	-36.0	6.0	0.0	0.4	24.4
	2225	- 0.4	13.7	49.0	3.5	- 8.3	-89.0	--	-45.0	7.5	0.0	0.5	30.5
2	445	7.1	- 3.9	9.2	0.8	1.3	36.7	--	- 9.0	1.5	0.0	0.1	6.1
	890	5.5	- 0.4	19.2	- 6.0	-25.6	45.7	--	-18.0	3.0	0.0	0.2	12.2
	1335	4.4	3.0	29.0	2.4	- 3.8	37.7	--	-27.0	4.5	0.0	0.3	18.3
	1780	3.8	8.0	38.7	3.4	- 5.8	37.9	--	-36.0	6.0	0.0	0.4	24.4
	2225	3.4	13.5	49.0	4.2	- 7.5	38.2	--	-45.0	7.5	0.0	0.5	30.5
	2670	4.7	18.4	59.4	5.3	- 7.1	37.7	--	-54.0	9.0	0.0	0.6	36.6
	3115	17.0	29.7	71.8	3.5	- 7.7	38.4	--	-63.0	10.5	0.0	0.7	42.7

TABLE 9 RESULTS VERSUS ANALYSIS - GAGES 25-27 AND 58-60

		RESULTS						ANALYSIS					
		FRONT			BACK			VIERENDEEL TRUSS			PLANE STRESS		
Day	Load (kN)	σ_x (MPa)	σ_y (MPa)	τ_{xy} (MPa)	σ_x (MPa)	σ_y (MPa)	τ_{xy} (MPa)	σ_x (MPa)	σ_y (MPa)	τ_{xy} (MPa)	σ_x (MPa)	σ_y (MPa)	τ_{xy} (MPa)
1	445	- 6.2	- 19.9	13.9	- 9.0	- 19.0	15.0	--	- 23.4	10.1	0.2	0.1	6.1
	890	-11.5	- 44.6	30.9	-20.4	- 43.8	34.6	--	- 46.8	20.2	0.4	0.2	12.2
	1335	-16.8	- 68.4	48.2	-31.1	- 68.9	54.0	--	- 70.2	30.3	0.6	0.3	18.3
	1780	-22.3	- 92.5	65.7	-39.1	- 95.2	72.5	--	- 93.6	40.4	0.8	0.4	24.4
	2225	-27.7	-111.8	82.8	-45.9	-117.3	88.3	--	-117.0	50.5	1.0	0.5	30.5
2	445	0.8	- 14.1	13.1	0.9	- 22.5	10.4	--	- 23.4	10.1	0.2	0.1	6.1
	890	- 6.2	- 39.3	31.1	-11.2	- 47.9	30.2	--	- 46.8	20.2	0.4	0.2	12.2
	1335	-13.5	- 63.4	48.2	-22.4	- 71.8	49.1	--	- 70.2	30.3	0.6	0.3	18.3
	1780	-21.1	- 88.3	66.1	-33.5	- 95.9	68.8	--	- 93.6	40.4	0.8	0.4	24.4
	2225	-29.7	-113.2	84.2	-45.0	-120.1	88.3	--	-117.0	50.5	1.0	0.5	30.5
	2670	-36.8	-133.9	100.7	-53.2	-142.1	105.6	--	-140.4	60.6	1.2	0.6	36.6
	3115	-15.5	-126.3	103.5	-54.3	-185.6	107.0	--	-117.0	70.7	1.4	0.7	42.7

TABLE 10 RESULTS VERSUS ANALYSIS - GAGES 28-30 AND 61-63

		RESULTS						ANALYSIS					
		FRONT			BACK			VIERENDEEL TRUSS			PLANE STRESS		
Day	Load (kN)	σ_x (MPa)	σ_y (MPa)	τ_{xy} (MPa)	σ_x (MPa)	σ_y (MPa)	τ_{xy} (MPa)	σ_x (MPa)	σ_y (MPa)	τ_{xy} (MPa)	σ_x (MPa)	σ_y (MPa)	τ_{xy} (MPa)
1	445	- 25.1	- 3.6	6.8	- 17.9	0.2	3.2	- 22.0	--	12.5	0.6	-0.2	6.0
	890	- 52.9	- 8.0	15.0	- 35.4	2.0	5.2	- 44.0	--	25.0	1.2	-0.4	12.0
	1335	- 76.6	-11.7	23.0	- 56.0	2.2	7.8	- 66.0	--	37.5	1.8	-0.6	18.0
	1780	- 96.6	-13.7	23.9	- 73.1	2.0	9.7	- 88.0	--	50.0	2.4	-0.8	24.0
	2225	-120.1	-14.9	16.2	- 89.7	4.4	12.1	-110.0	--	62.5	3.0	-1.0	30.0
2	445	23.8	- 7.0	-14.1	14.9	11.7	-15.5	- 22.0	--	12.5	0.6	-0.2	6.0
	890	- 11.6	-10.3	- 4.8	- 17.6	8.4	- 7.4	- 44.0	--	25.0	1.2	-0.4	12.0
	1335	- 47.5	-12.8	3.8	- 49.3	5.3	0.7	- 66.0	--	37.5	1.8	-0.6	18.0
	1780	- 81.4	-14.1	8.6	- 78.0	3.2	8.4	- 88.0	--	50.0	2.4	-0.8	24.0
	2225	-117.3	-15.0	7.6	-118.7	- 1.4	21.6	-110.0	--	62.5	3.0	-1.0	30.0
	2670	-152.5	-18.0	- 4.5	-149.7	1.6	30.5	-132.0	--	75.0	3.6	-1.2	36.0
	3115	-198.7	-26.2	-28.8	-178.7	9.2	36.3	-154.0	--	87.5	4.2	-1.4	42.0

TABLE 12 LOADING FRAME COLUMN GAGE READINGS

Day	Machine Load (kN)	Theoretical Column Load (kN)	Load @ Gage #69 (kN)	Percent of Total Column Load (%)	Gage #66 (kN)	Percent of Total Column Load (%)
1	0	0	0	0	0	0
	223	214	53	25	0	0
	445	427	218	51	40	9
	668	645	338	52	53	8
	890	859	449	52	62	7
	1113	1072	574	54	107	10
	1335	1286	708	55	169	13
	1558	1500	828	55	200	13
	1780	1713	966	56	263	15
	2003	1931	1099	57	316	16
2	445	427	n/a	n/a	45	10
	890	859	n/a	n/a	169	20
	1335	1286	n/a	n/a	276	21
	1780	1713	n/a	n/a	383	22
	2225	2140	n/a	n/a	507	23
	2670	2568	n/a	n/a	627	24

TABLE 13 WINDOW DIAGONAL ANALYSES AND RESULTS FOR FIRST LOADING

Window	Load (kN)	Diagonal Shortening (mm)	Diagonal Lengthening (mm)	Average Length Change (mm)	Predicted Length Change (mm)	Average Change / Predicted Change x 33-1/3% (%)	
3rd Floor	445	0.201	0.274	0.239	0.358	22	
	890	0.193	0.838	0.516	0.716	24	
	1335	0.221	1.455	0.838	1.074	26	
	1780	0.213	2.294	1.255	1.433	29	
						25	Average
2nd Floor	445	0.386	0.505	0.447	0.358	41	
	890	1.257	1.113	1.186	0.716	55	
	1335	1.961	1.783	1.872	1.074	57	
	1780	3.200	2.565	2.883	1.433	66	
						55	Average
1st Floor	445	0.442	0.499	0.470	0.358	43	
	890	1.049	1.112	1.082	0.716	50	
	1335	1.676	1.728	1.702	1.074	52	
	1780	2.022	2.412	2.217	1.433	51	
						49	Average
						129	Total

TABLE 14 WINDOW DIAGONAL ANALYSES AND RESULTS FOR SECOND LOADING

Window	Load (kN)	Diagonal Shortening (mm)	Diagonal Lengthening (mm)	Average Length Change (mm)	Predicted Length Change (mm)	$\frac{\text{Average Change}}{\text{Predicted Change}} \times 33\text{-}1/3\%$ (%)	
3rd Floor	223	0.000	0.000	0.000	0.000	0	
	445	0.175	0.315	0.246	0.358	23	
	1335	1.519	1.402	1.461	1.074	45	
	1780	2.174	2.002	2.088	1.433	48	
						39	Average
2nd Floor	223	0.000	0.000	0.000	0.000	0	
	445	0.366	0.450	0.409	0.358	38	
	1335	1.557	0.729	1.143	1.074	35	
	1780	2.215	1.321	1.768	1.433	41	
						38	Average
1st Floor	223	0.000	0.000	0.000	0.000	0	
	445	0.269	n/a	0.269	0.358	25	
	1335	1.306	1.128	1.217	1.074	37	
	1780	1.839	1.717	1.778	1.433	41	
						34	Average
						111	Total

TABLE 15 TEST RESULTS OF STIFFENER GAGES

Machine Load (kN)	Average Strain on Vertical Gages (micro-mm/mm)	Average Stress (MPa)	Stiffener Load (kN)
445	16	3.3	5.3
890	27	5.6	8.9
1335	36	7.5	12.0
1780	42	8.7	14.2
2225	47	9.7	15.6
2670	56	11.6	18.7
3115	588	121.7	196.2
3338	496	102.7	165.5

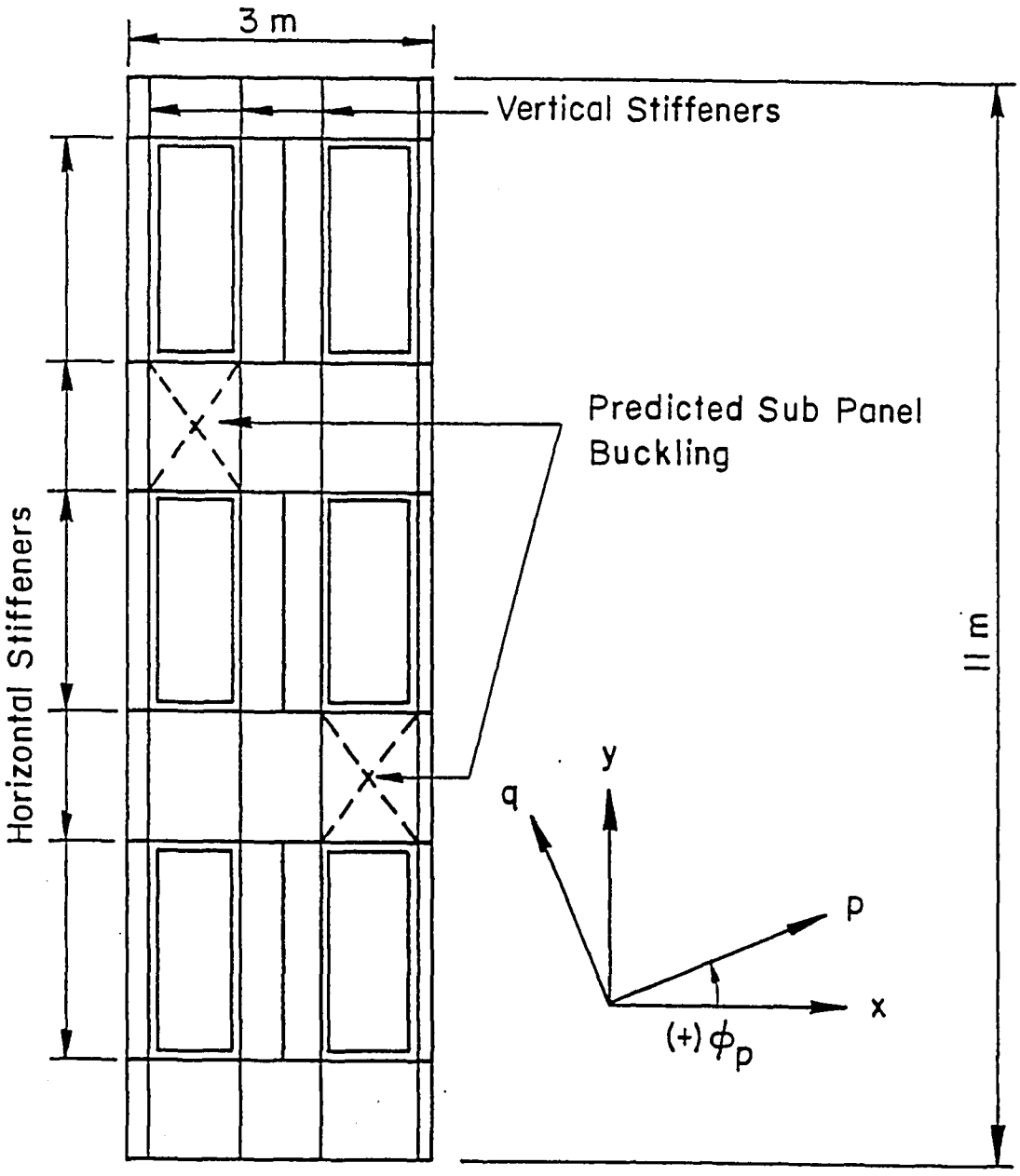

Fig. 1 Test Panel Schematic

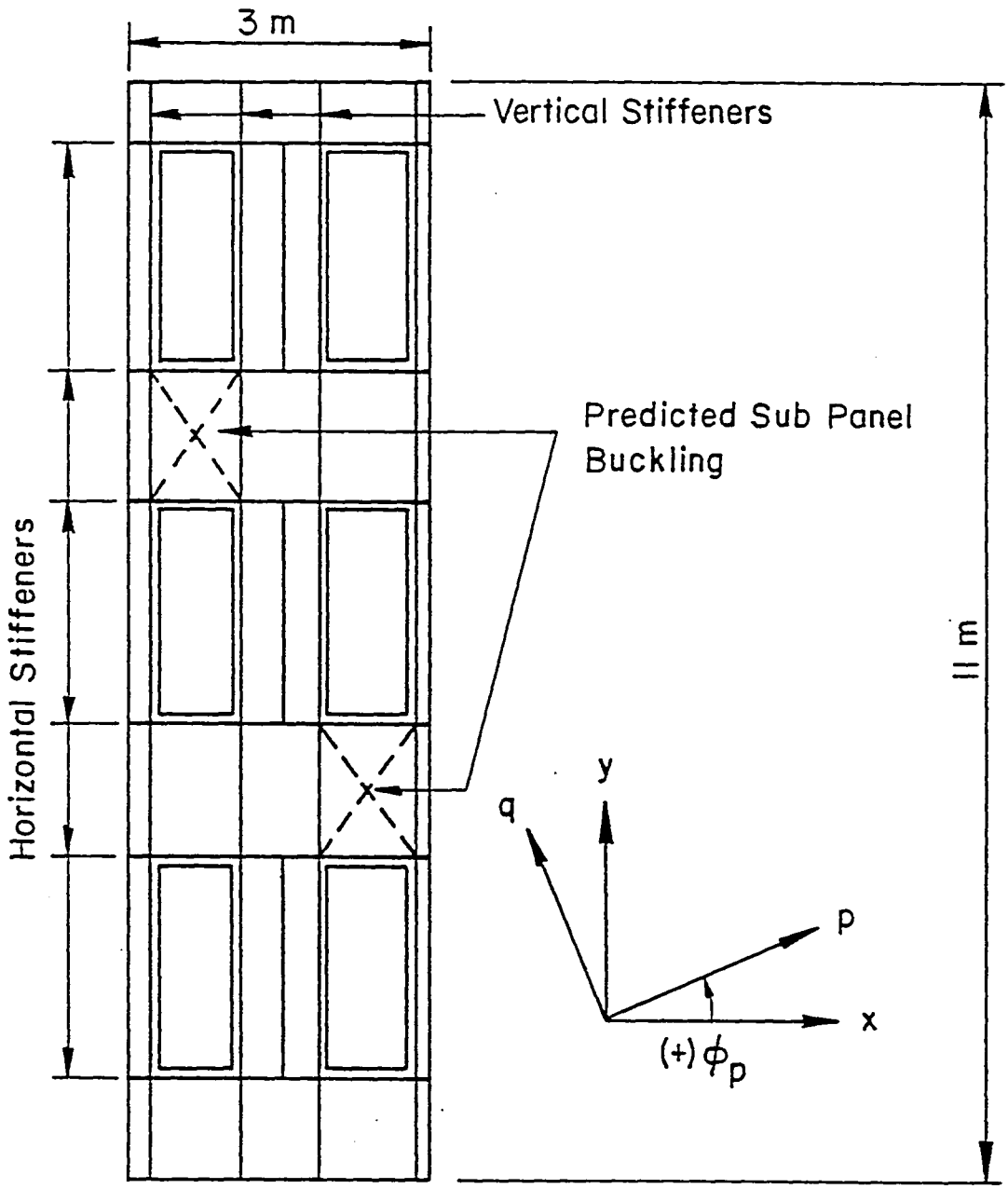

Fig. 1 Test Panel Schematic

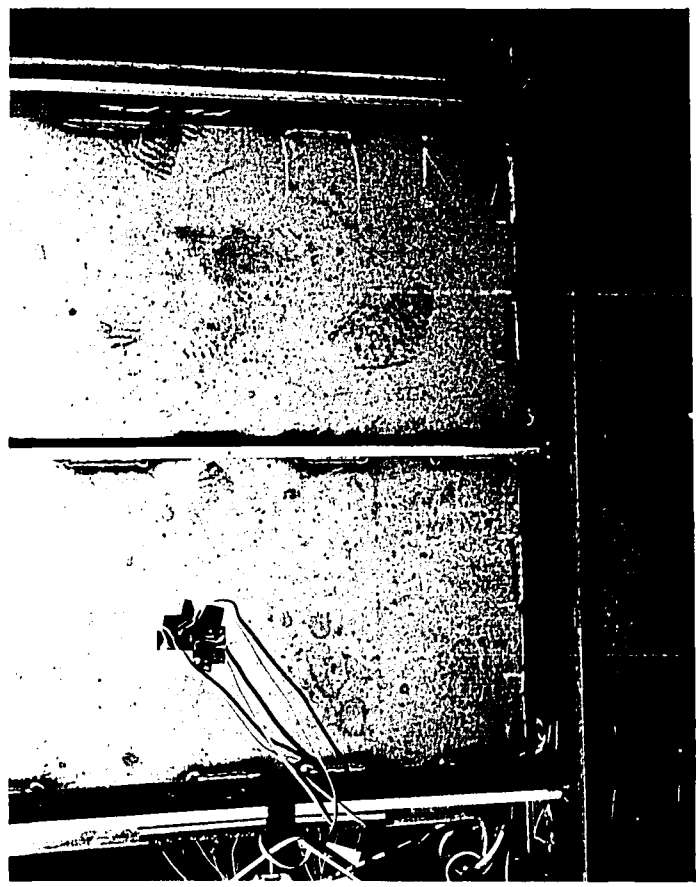

Fig. 2 Longitudinal and Transverse Stiffeners

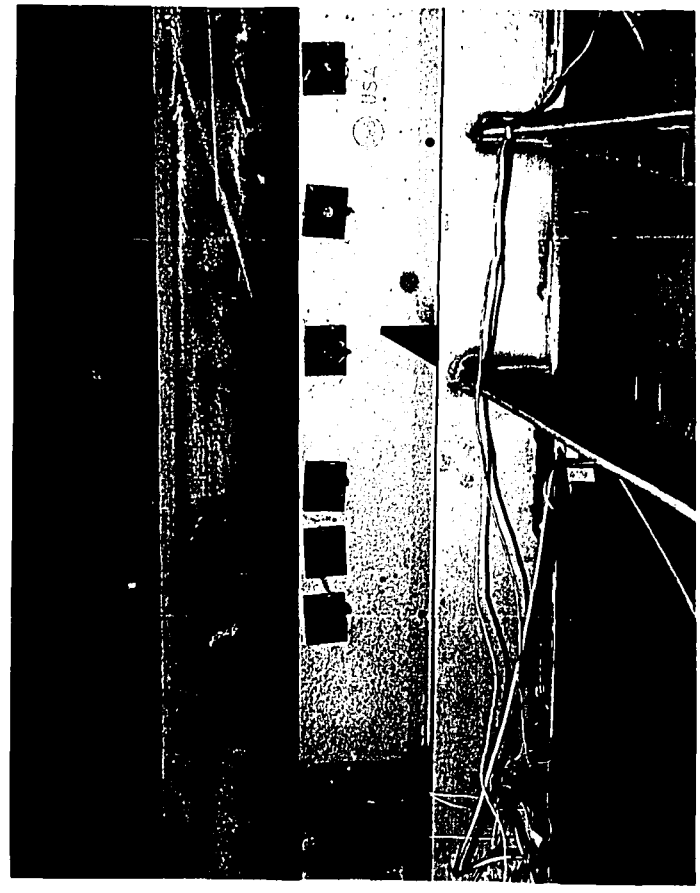

Fig. 3 Top Panel-to-Frame Connection

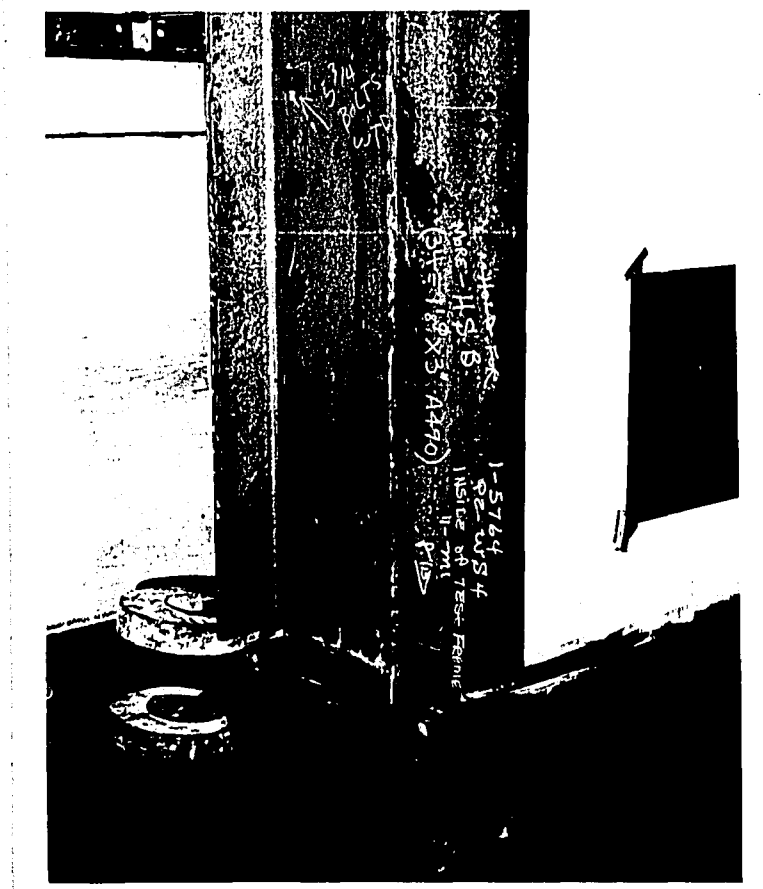

Fig. 4 Top Panel-to-Frame Connection

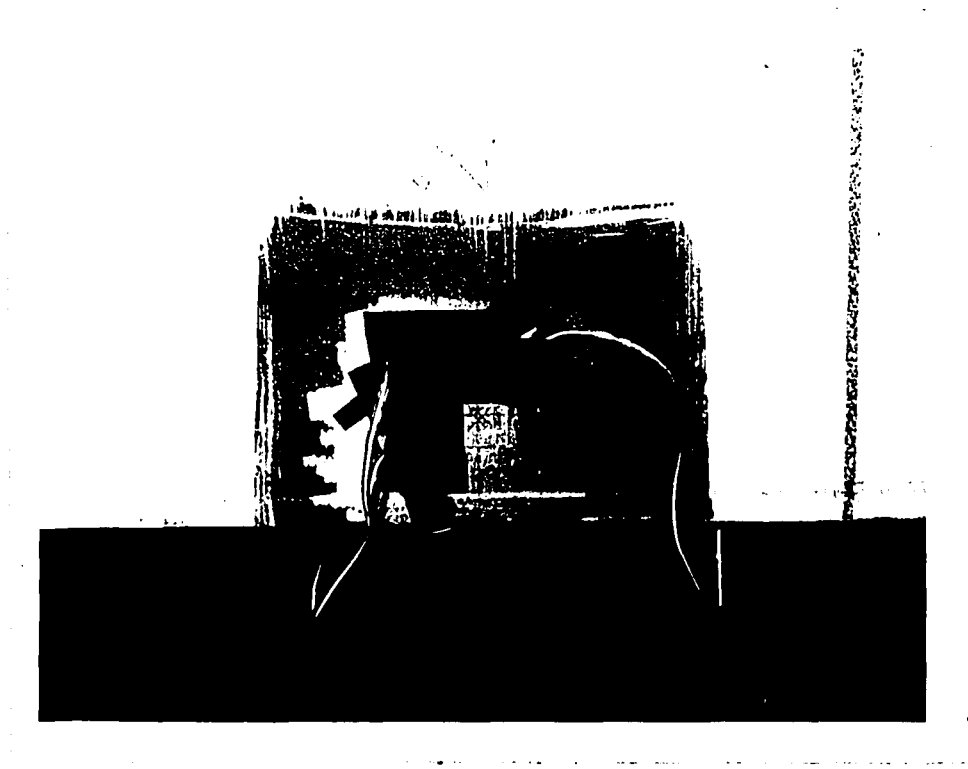

Fig. 5 Typical Strain Gage Mounting

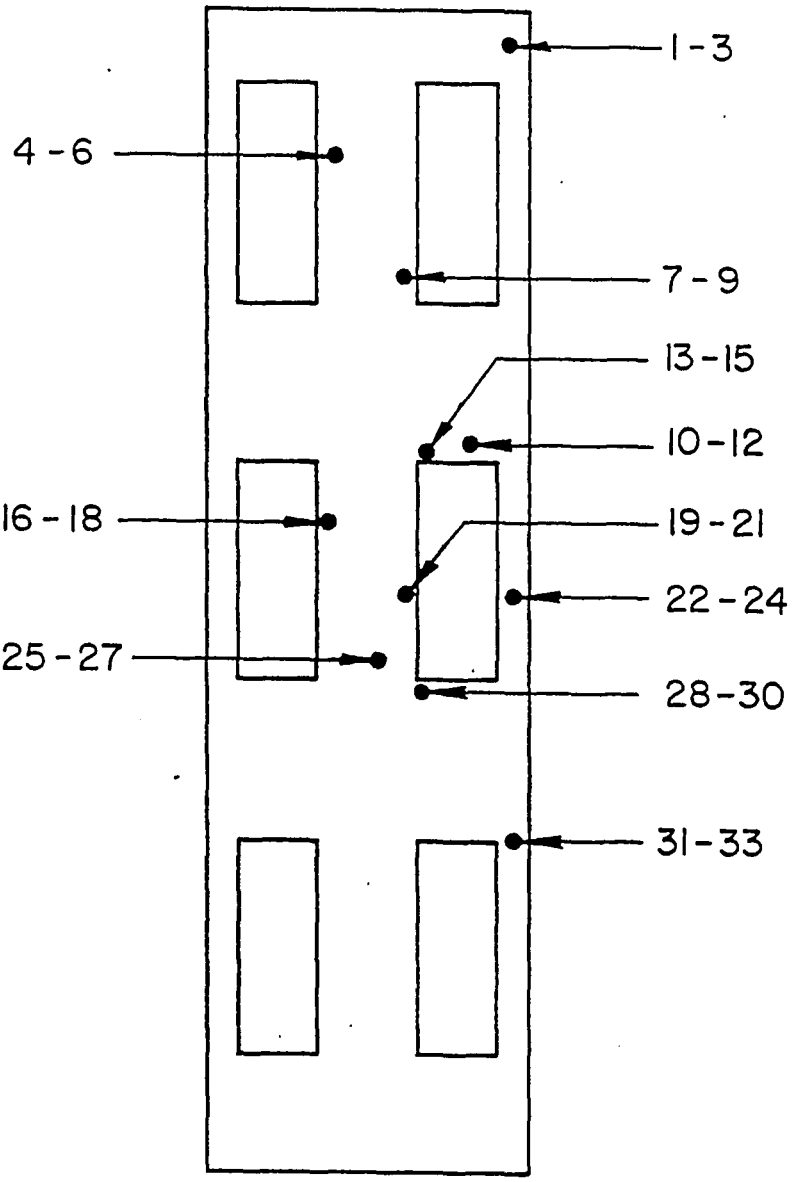

Note: The locations of gages 34-66 on the back side of the panel may be found by adding 33 to the above gage numbers.

Fig. 6 Panel Strain Gage Locations

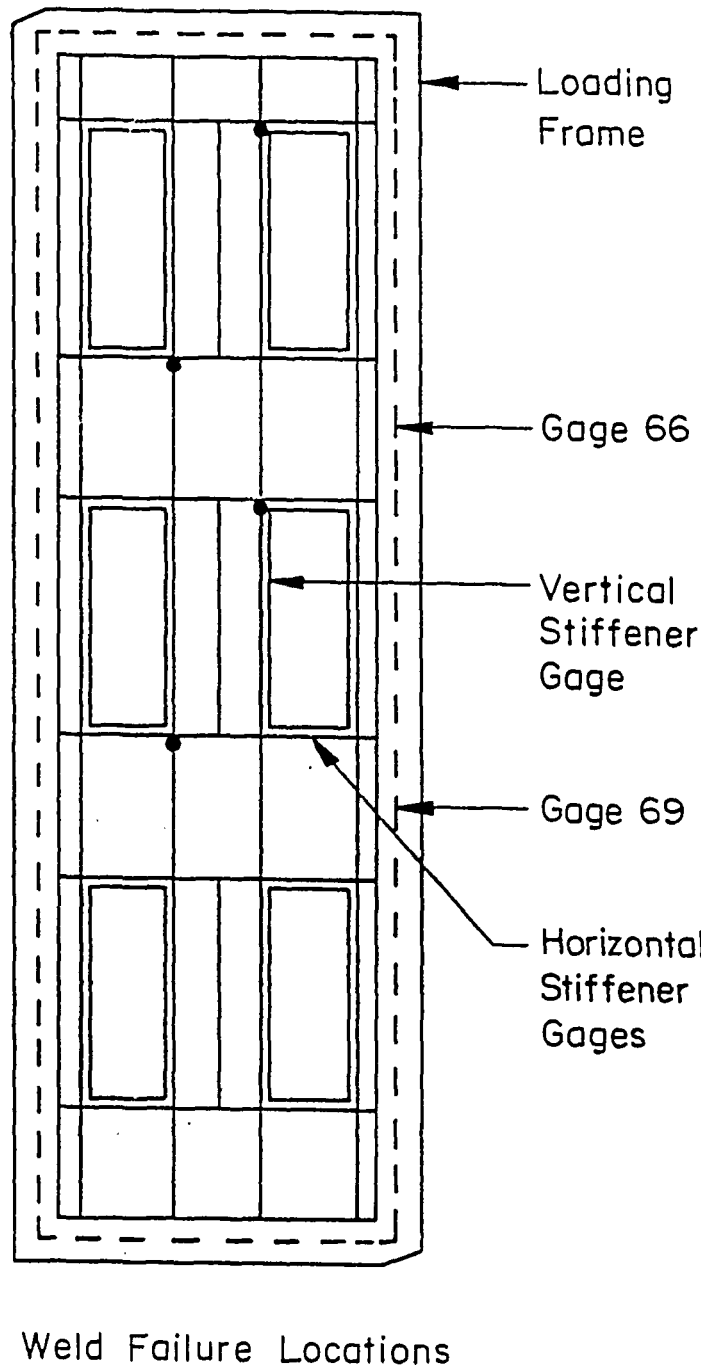

Fig. 7 Stiffener and Frame Strain Gage Locations

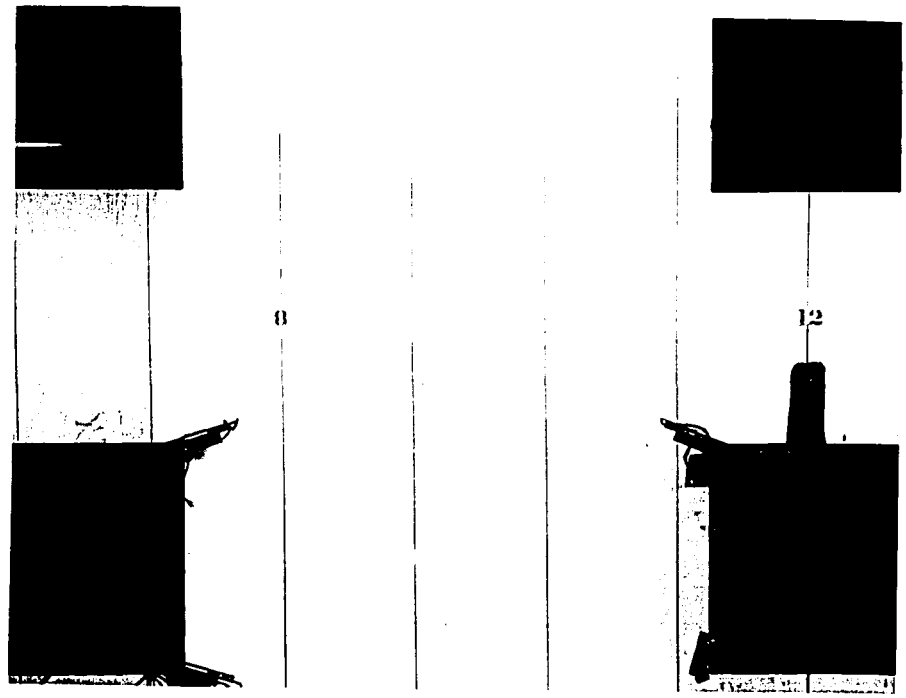

Fig. 8 Panel Grid Markings

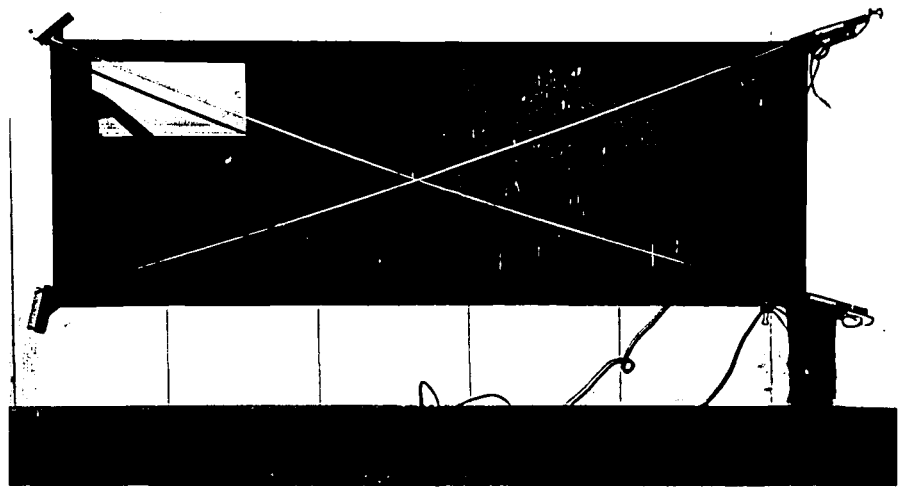

Fig. 9 Window Diagonal Rods and LVDT's

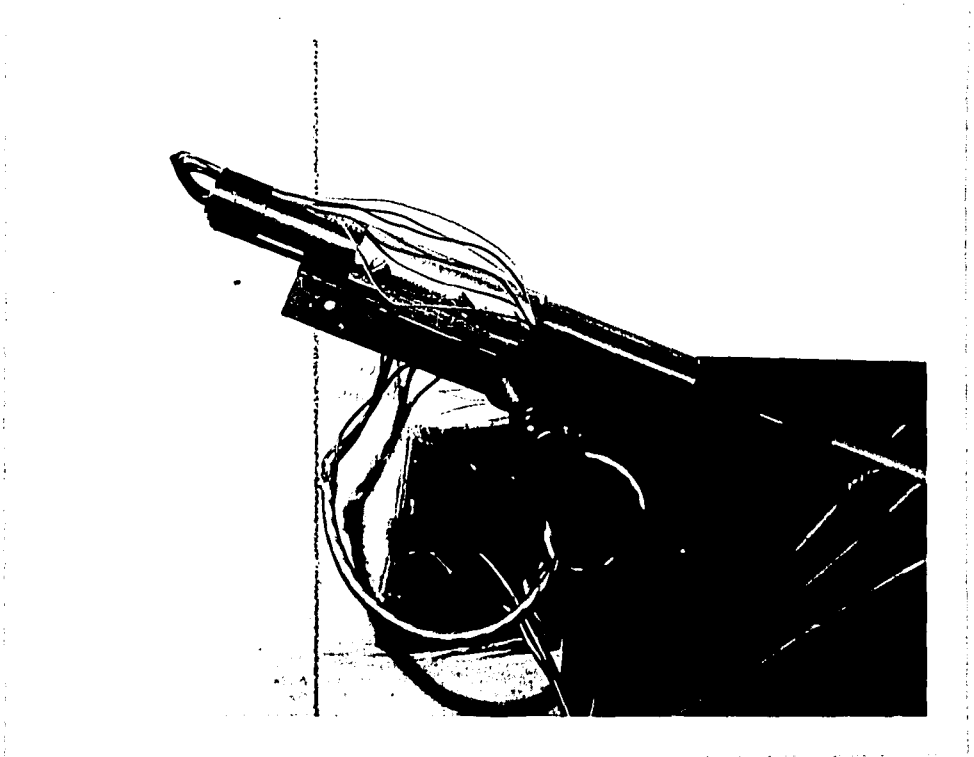

Fig. 10 Typical LVDT Mounting

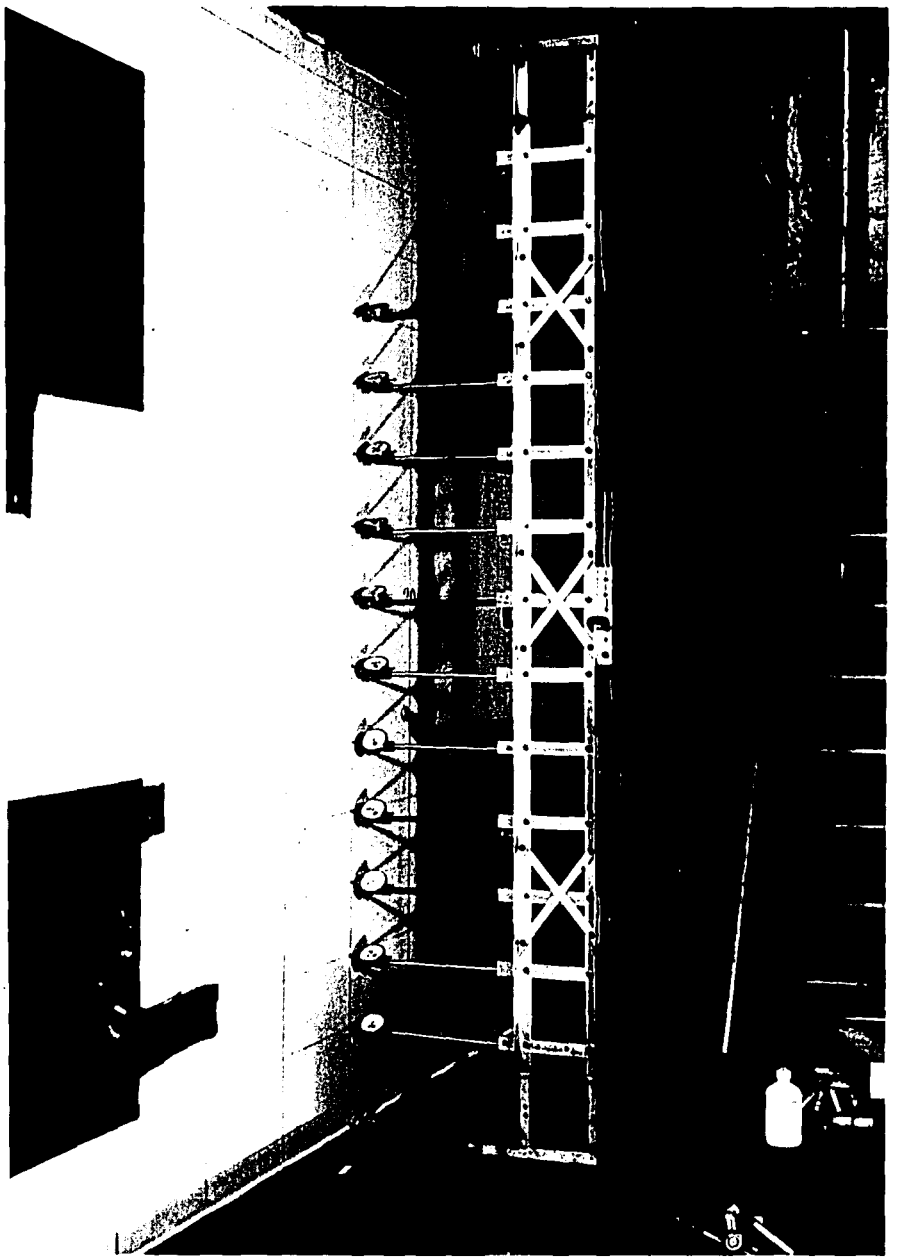

Fig. 11 Dial Gage Ladder

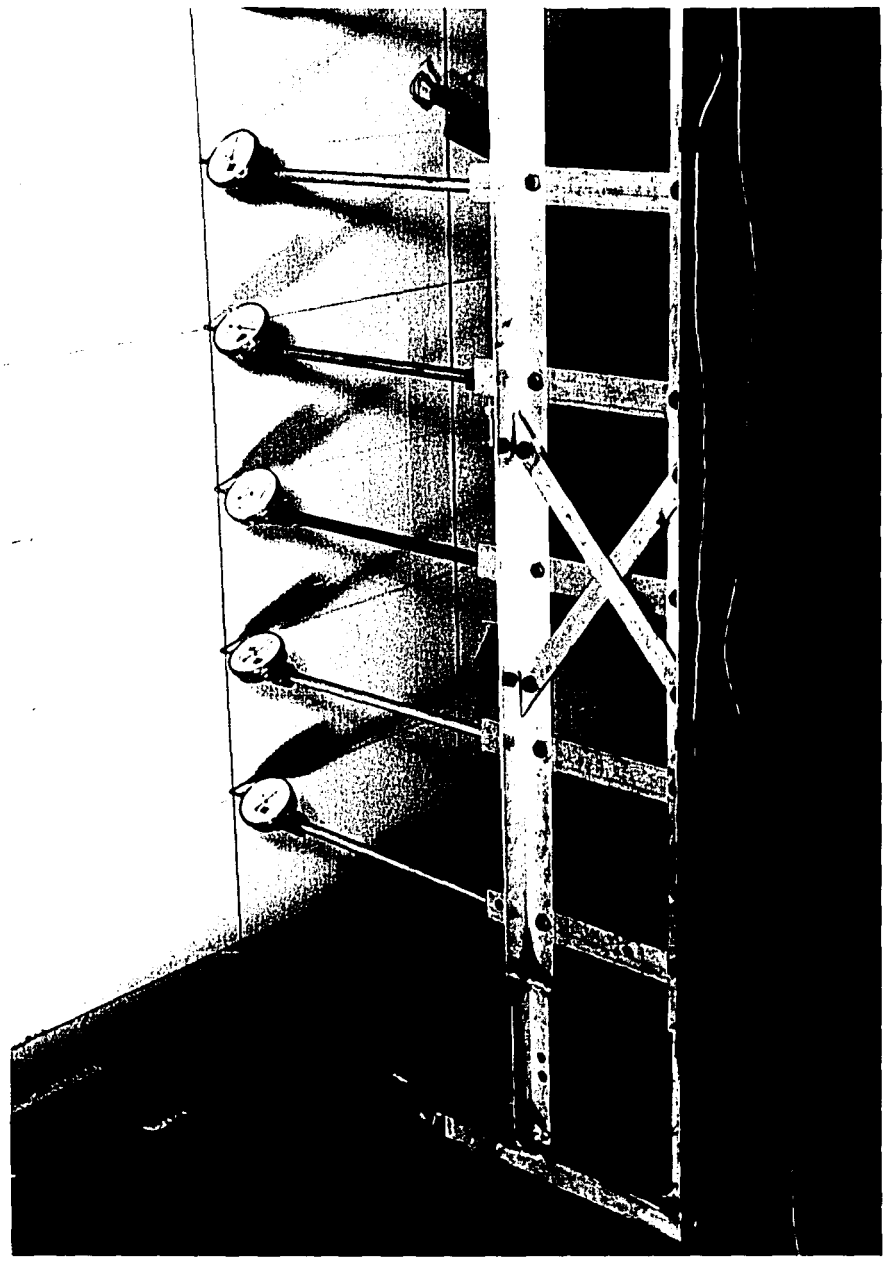

Fig. 12 Detail of Dial Gage Ladder and Grid Points

Fig. 13 Panel Lifting Arrangement

Fig. 13 Panel Lifting Arrangement

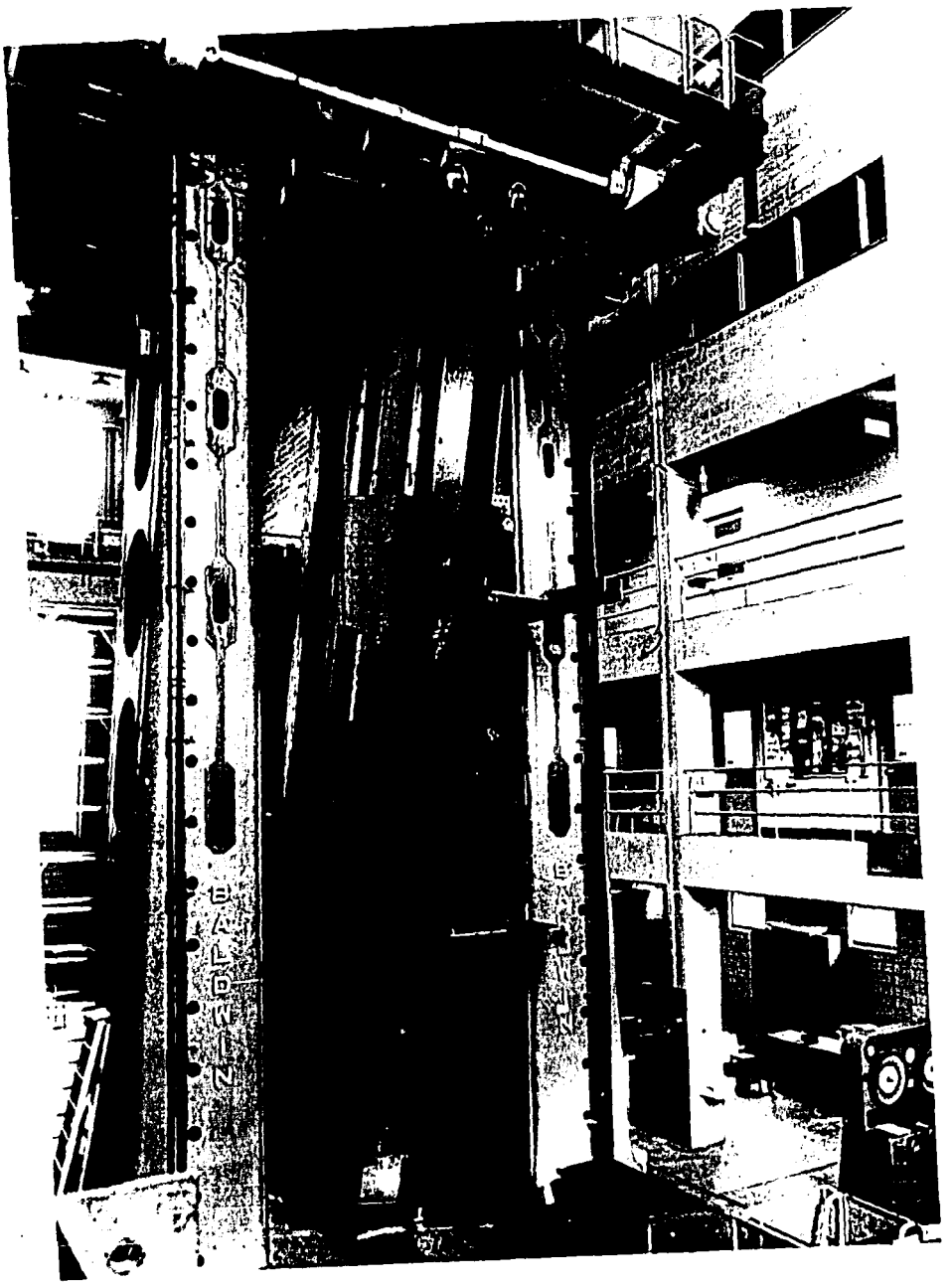

Fig. 14 Panel Positioned in Testing Machine

Fig. 15 Racking Deflection
Measurement Devices

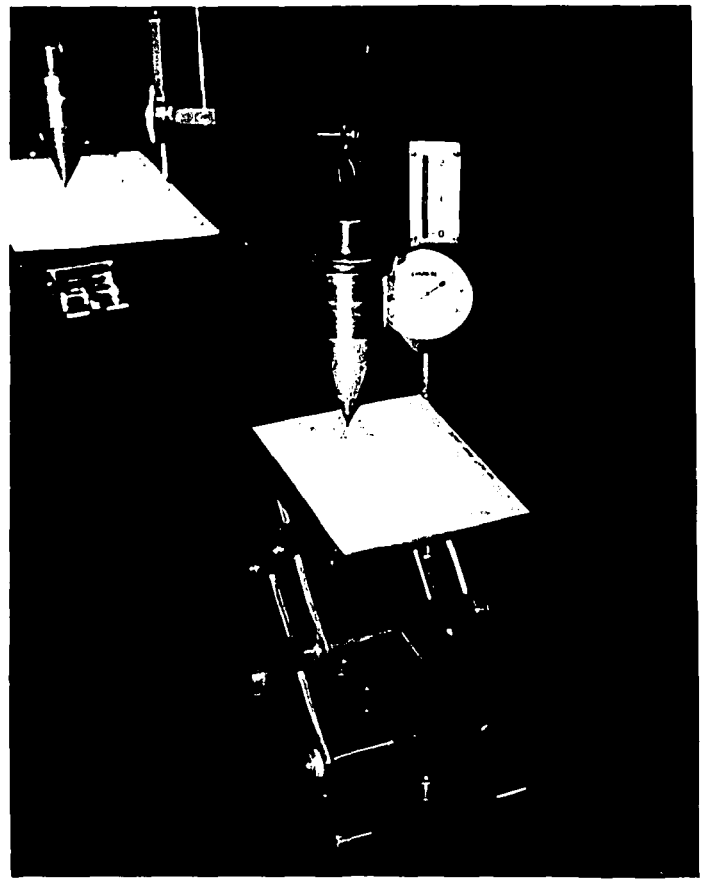

Fig. 16 Plumb Bob and Lab Table Detail

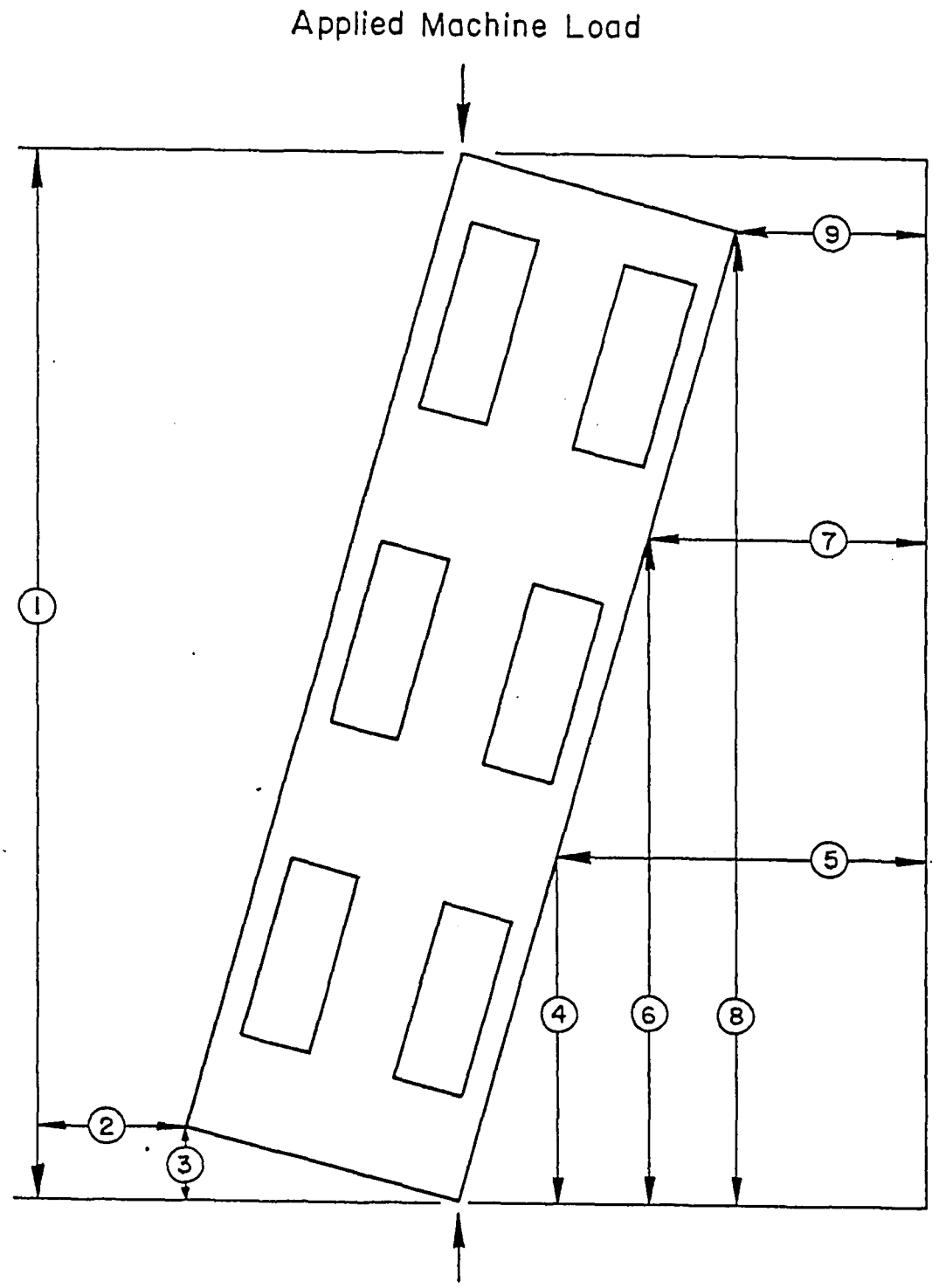

Fig. 17 In-plane Deformation Measurements

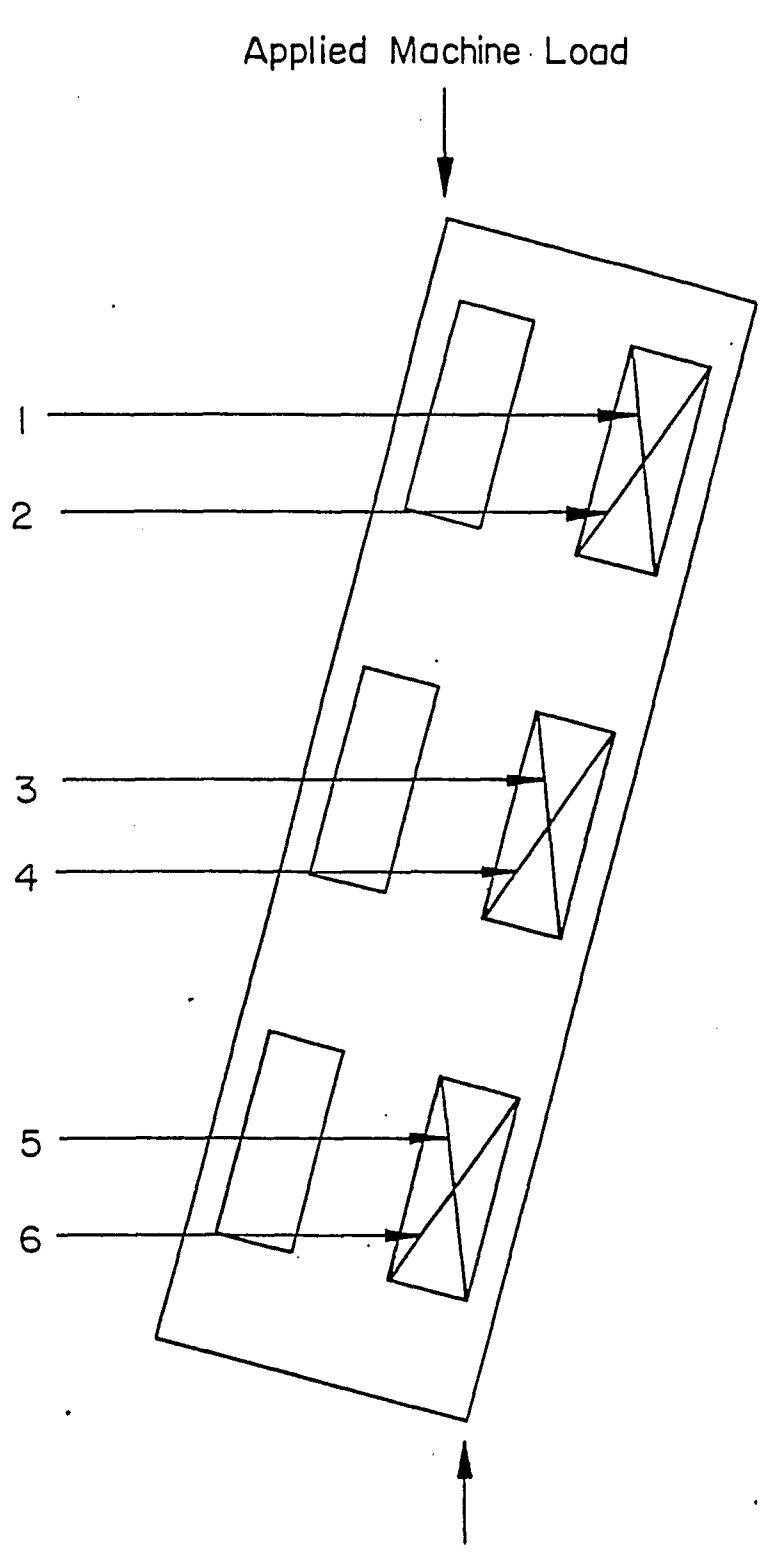

Fig. 18 Window Diagonal Deformation Measurements

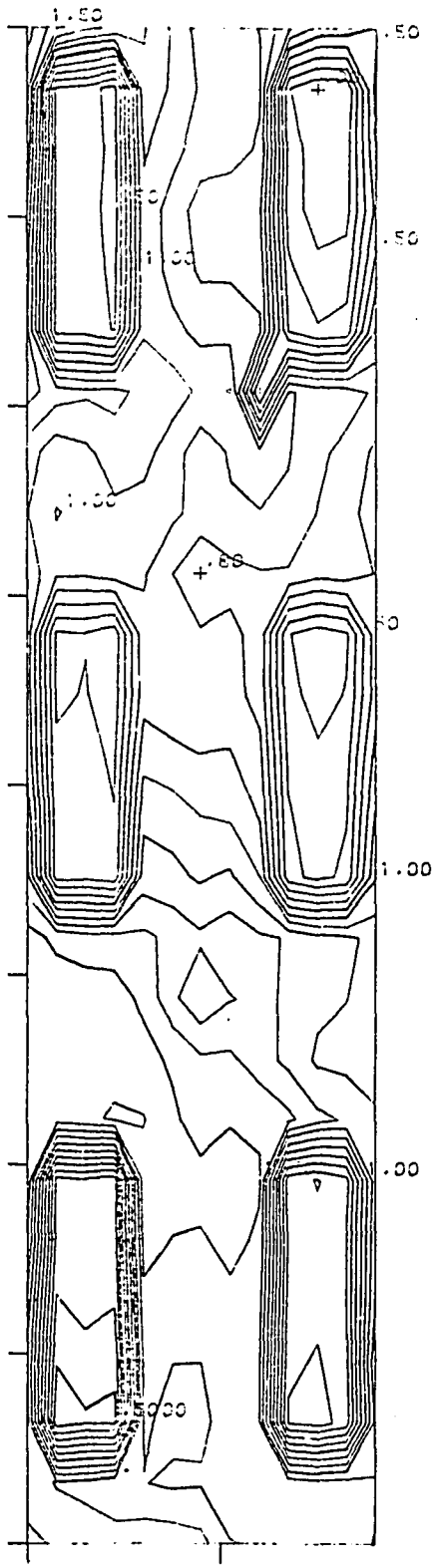

Fig. 19 Initial Panel Contours (No Load)

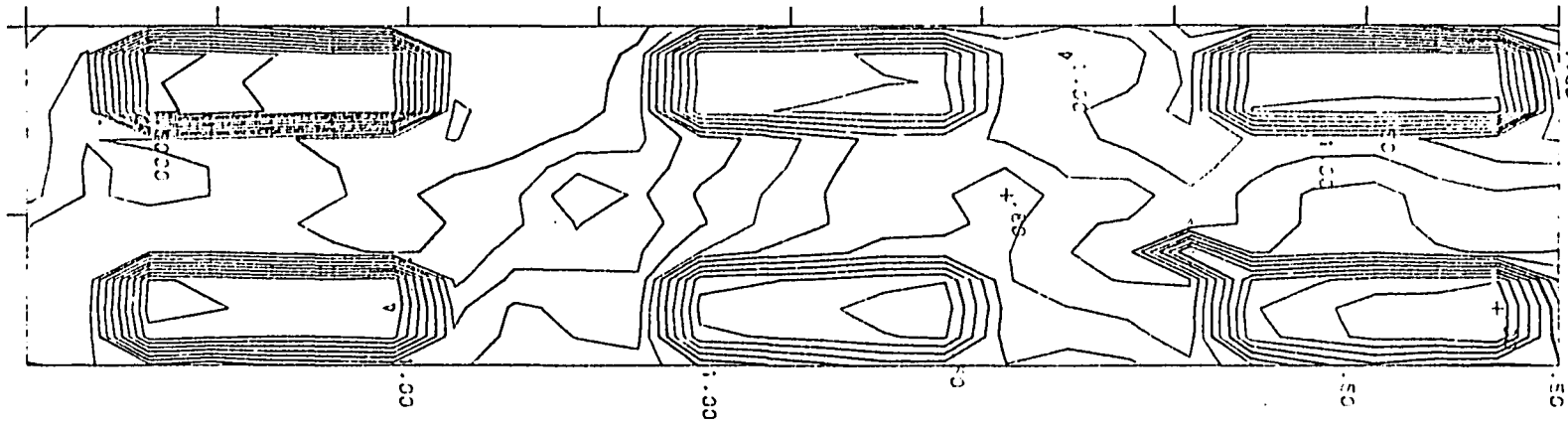

Fig. 19 Initial Panel Contours (No Load)

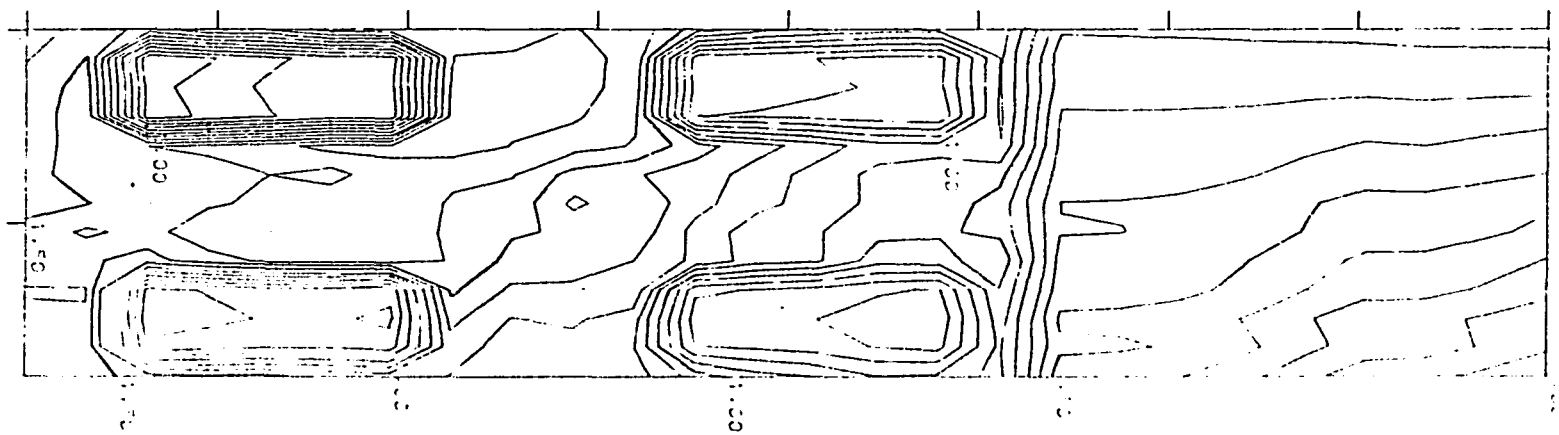

Fig. 20 Panel Contours at 107 kN (24^{k})

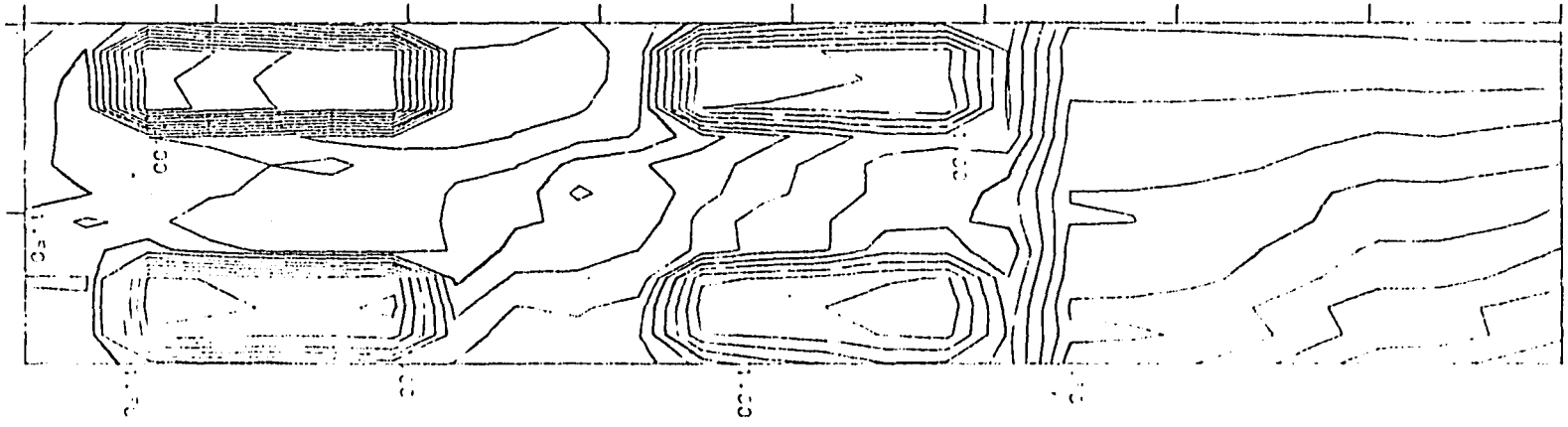

Fig. 20 Panel Contours at 107 kN (24^{k})

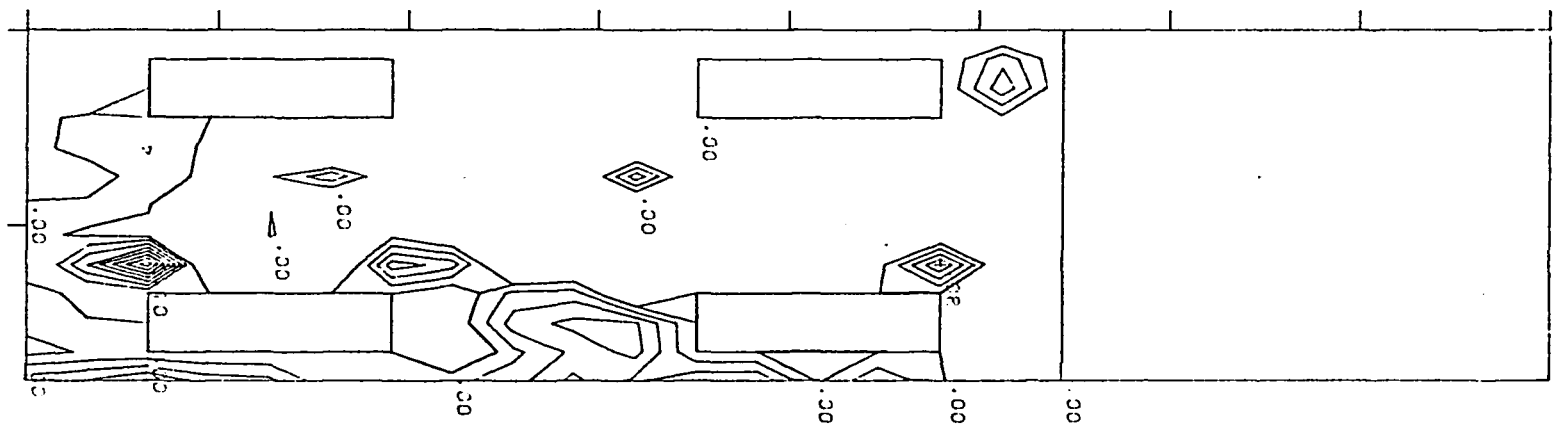

Fig. 21 Panel Contours at 1.34 MN (300^{k})

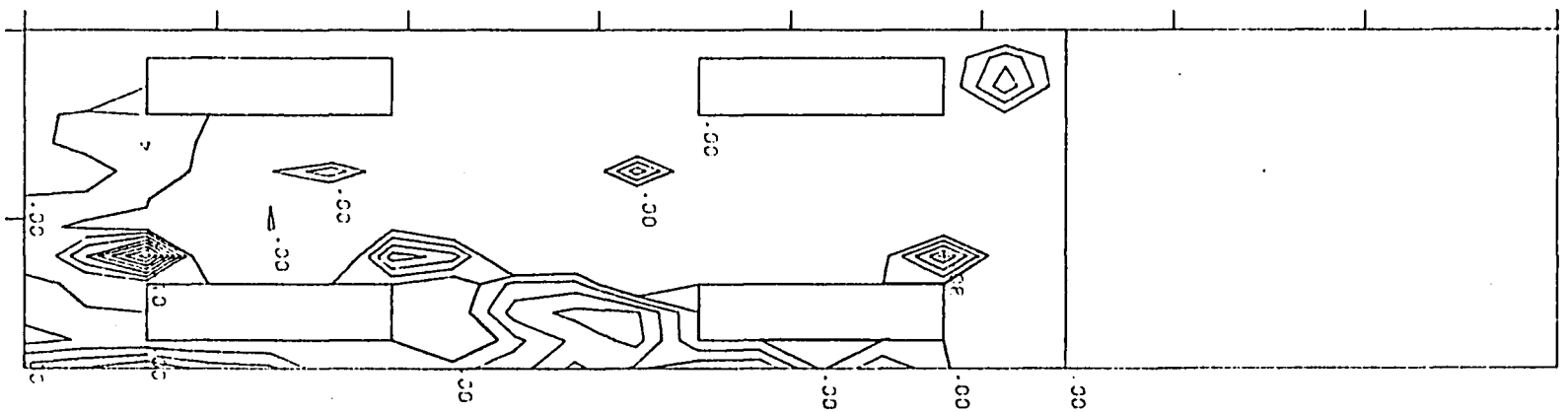

Fig. 21 Panel Contours at 1.34 MN (300^{k})

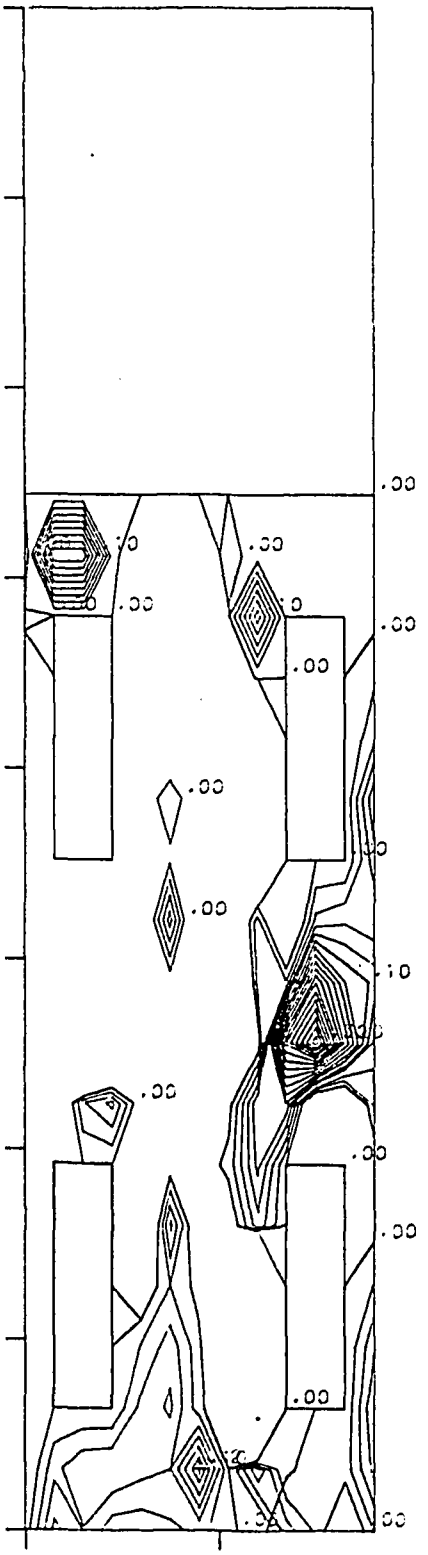

Fig. 22 Panel Contours at 2.45 MN (550^{k})

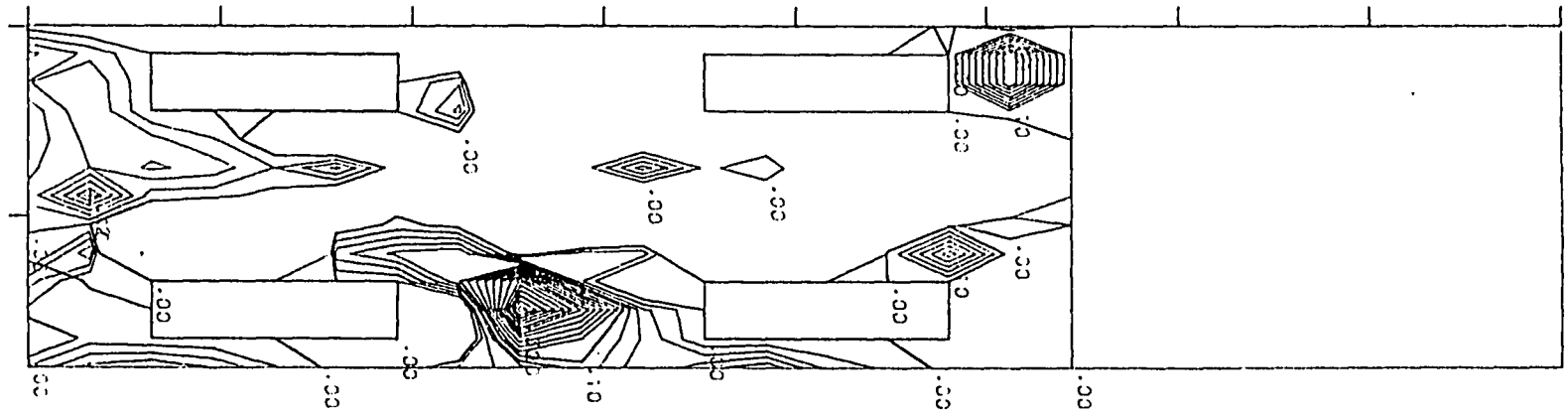

Fig. 22 Panel Contours at 2.45 MN (550^{k})

Fig. 23 Typical Weld Failure

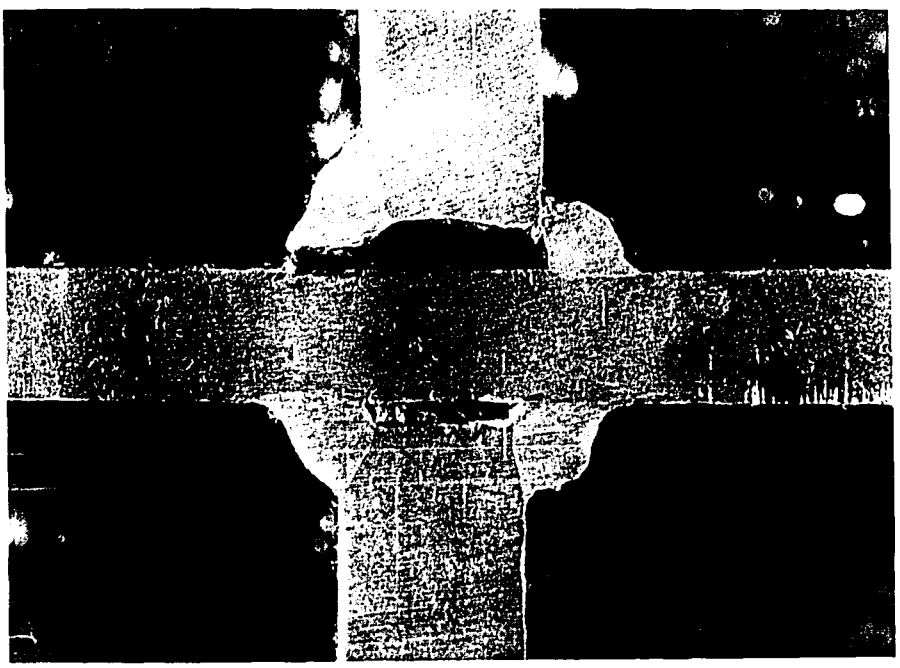

Fig. 24 Cross-section of Weld Failure

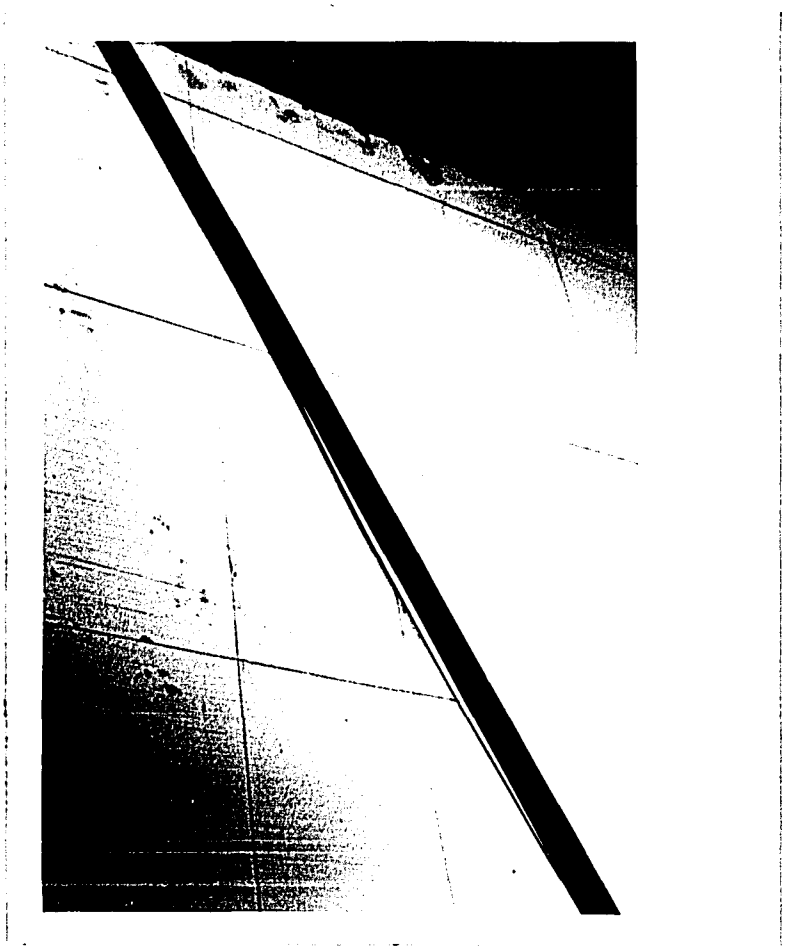

Fig. 25 Sub-panel Out-of-Plane Deformation

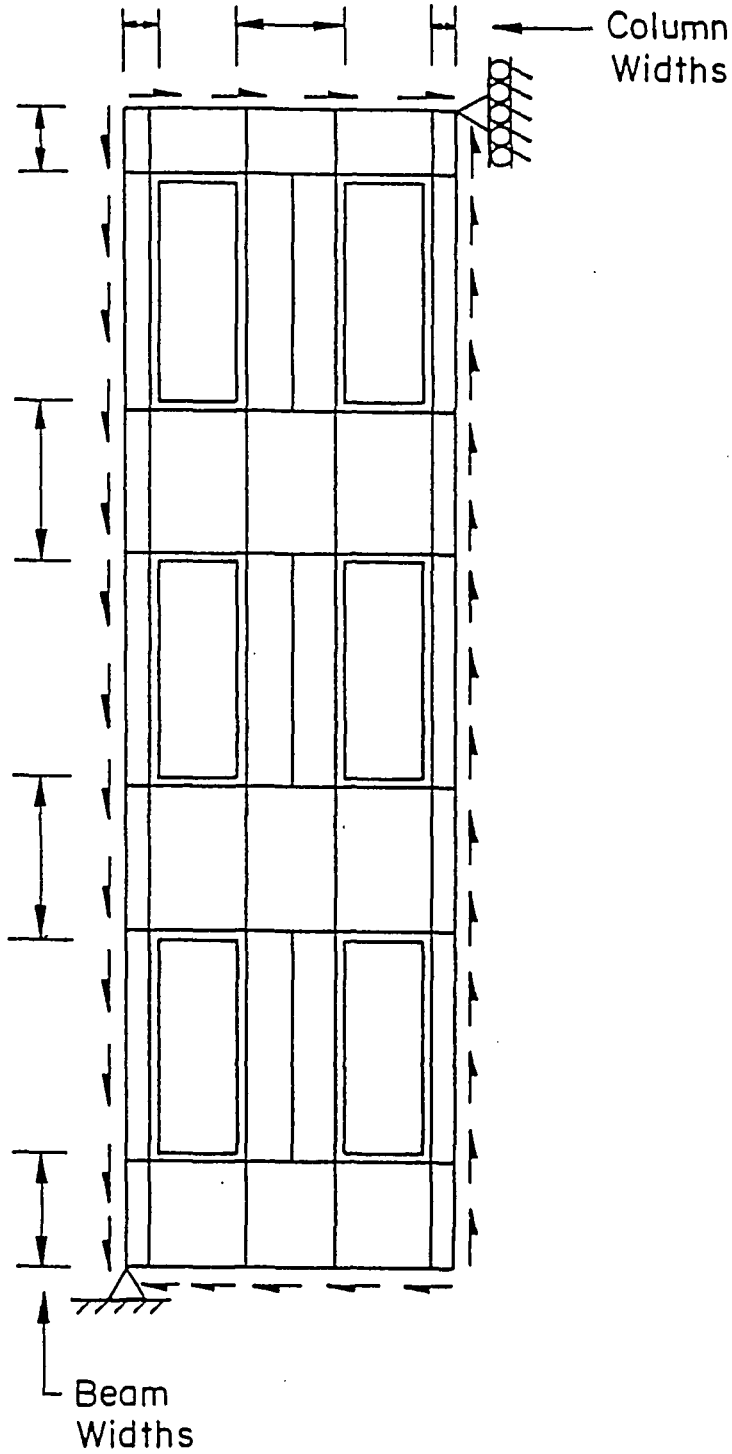

Fig. 26 Vierendeel Truss Model Showing Full Member Widths

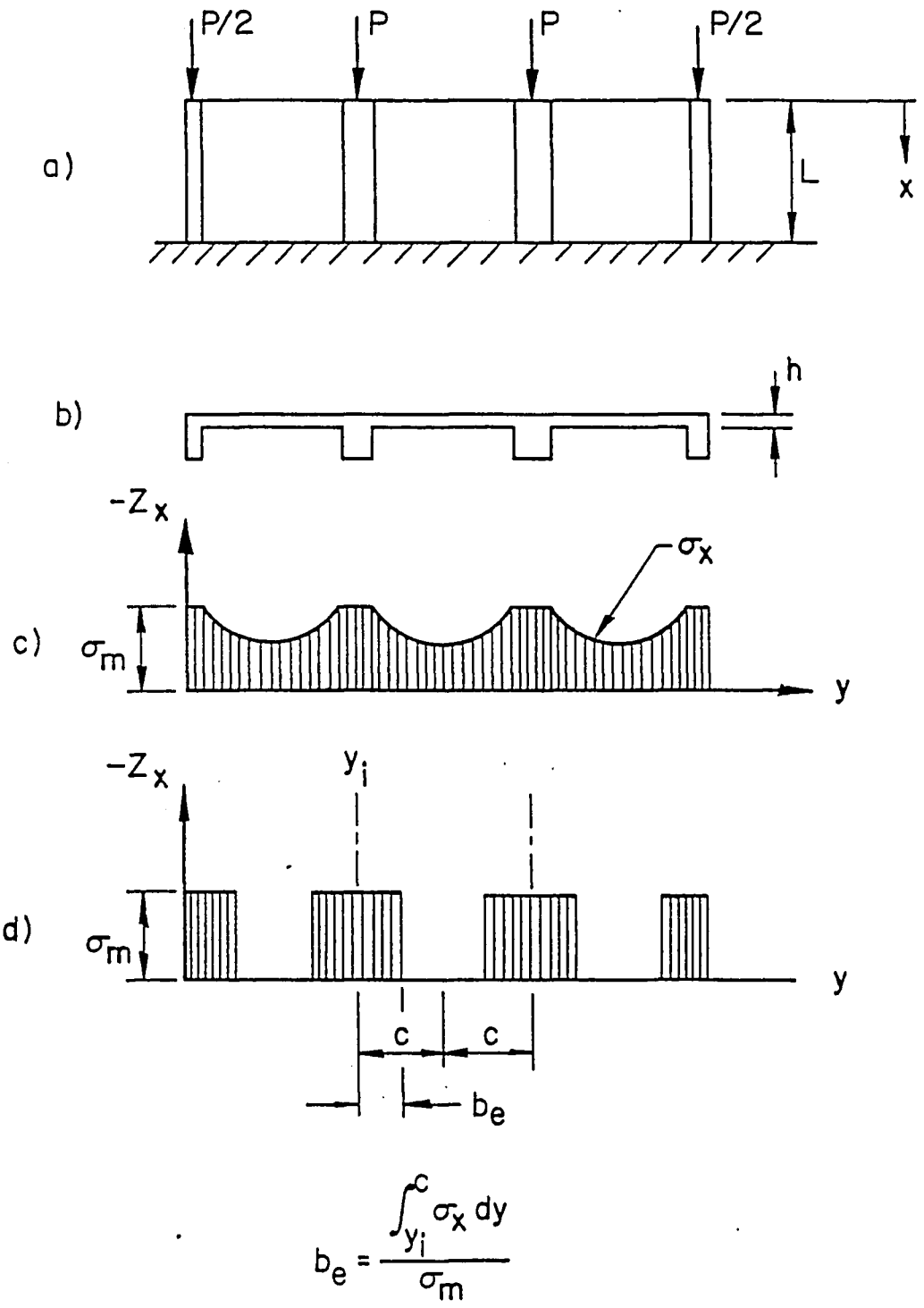

$$b_e = \frac{\int_{y_i}^{c} \sigma_x \, dy}{\sigma_m}$$

Fig. 27 Effective Width Concept; (a) Structure subjected to concentrated loading, (b) Ribbed cross-section, (c) Actual stress distribution, and (d) Stress distribution using the effective width concept.

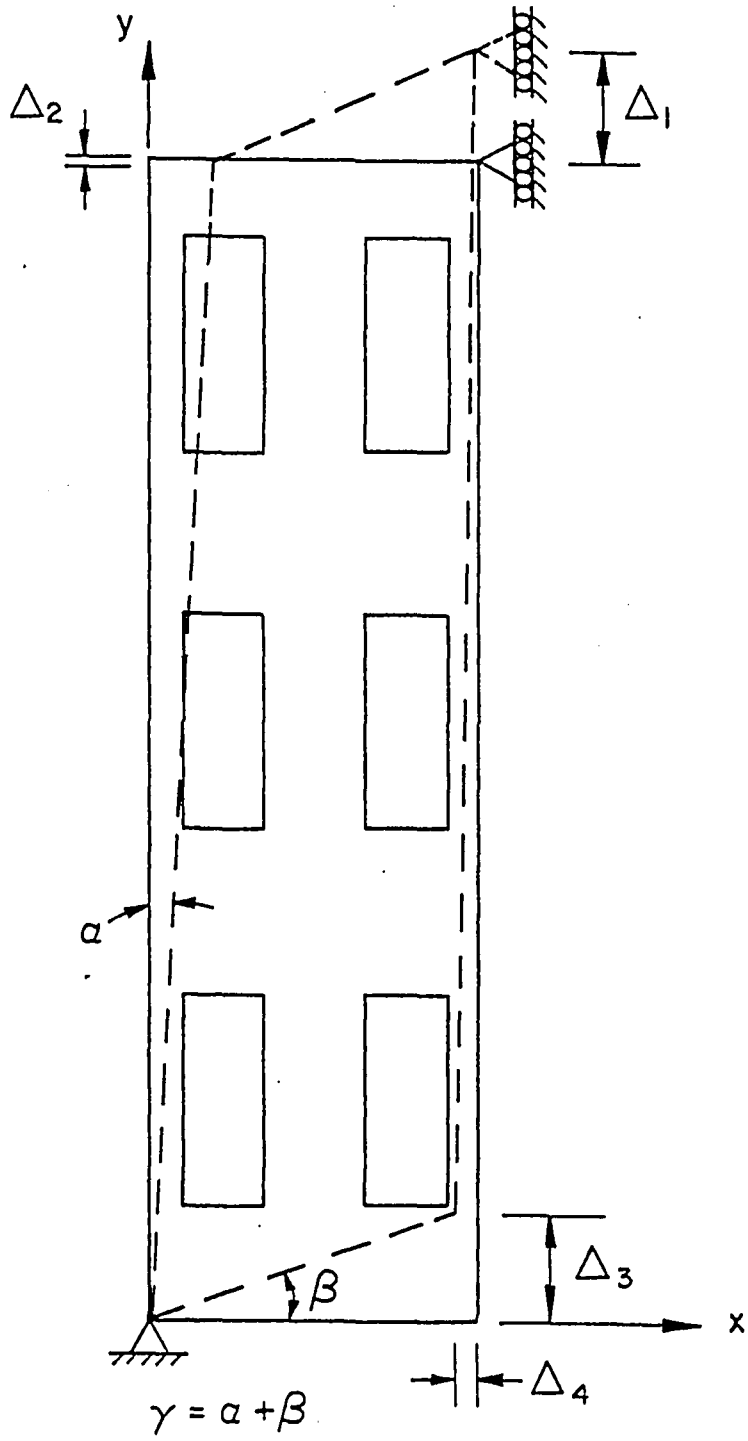

Fig. 28 Vierendeel Truss Analysis Deformations

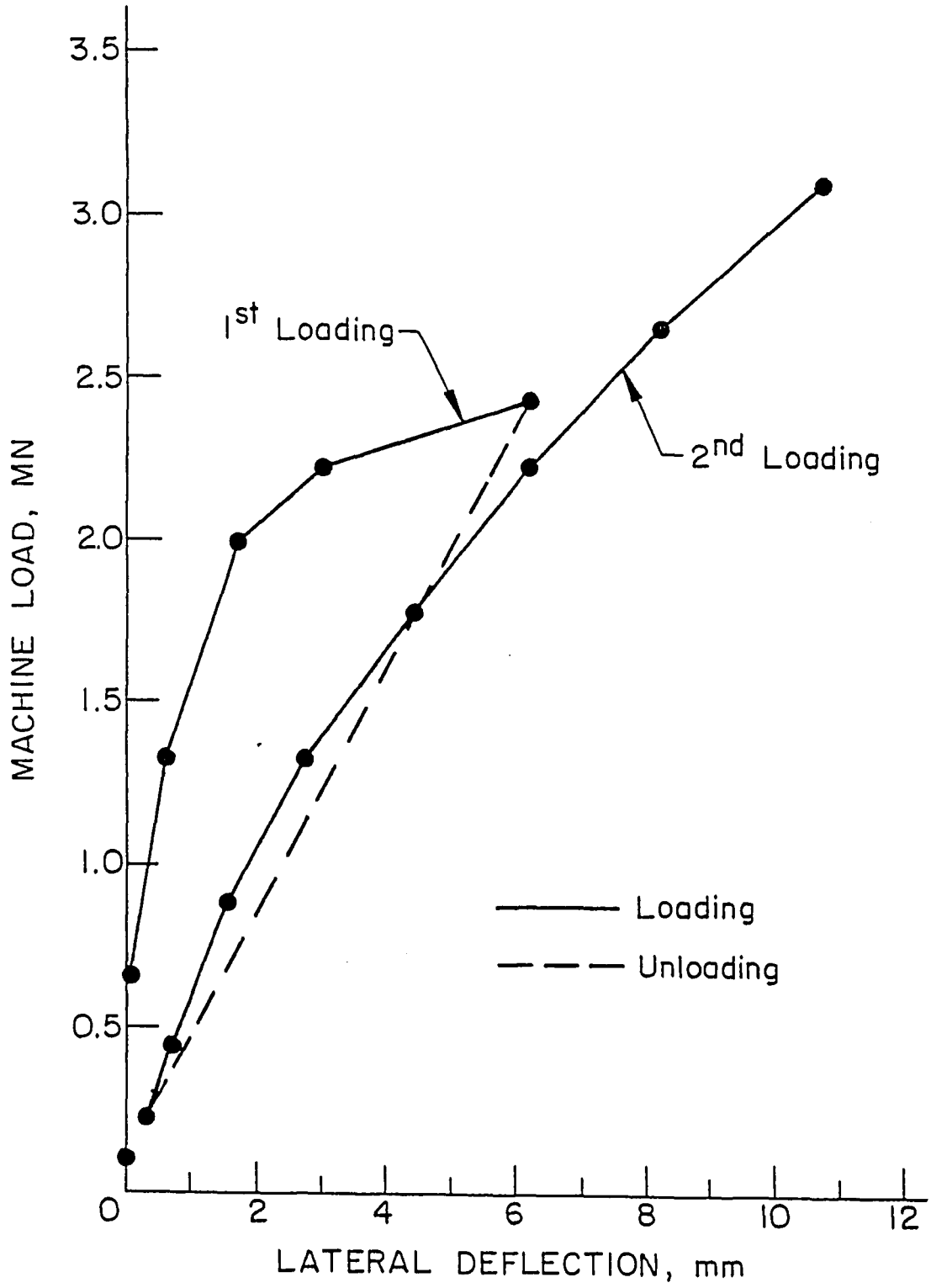

Fig. 29 Critical Sub-Panel Region Grid Point (9, 10)

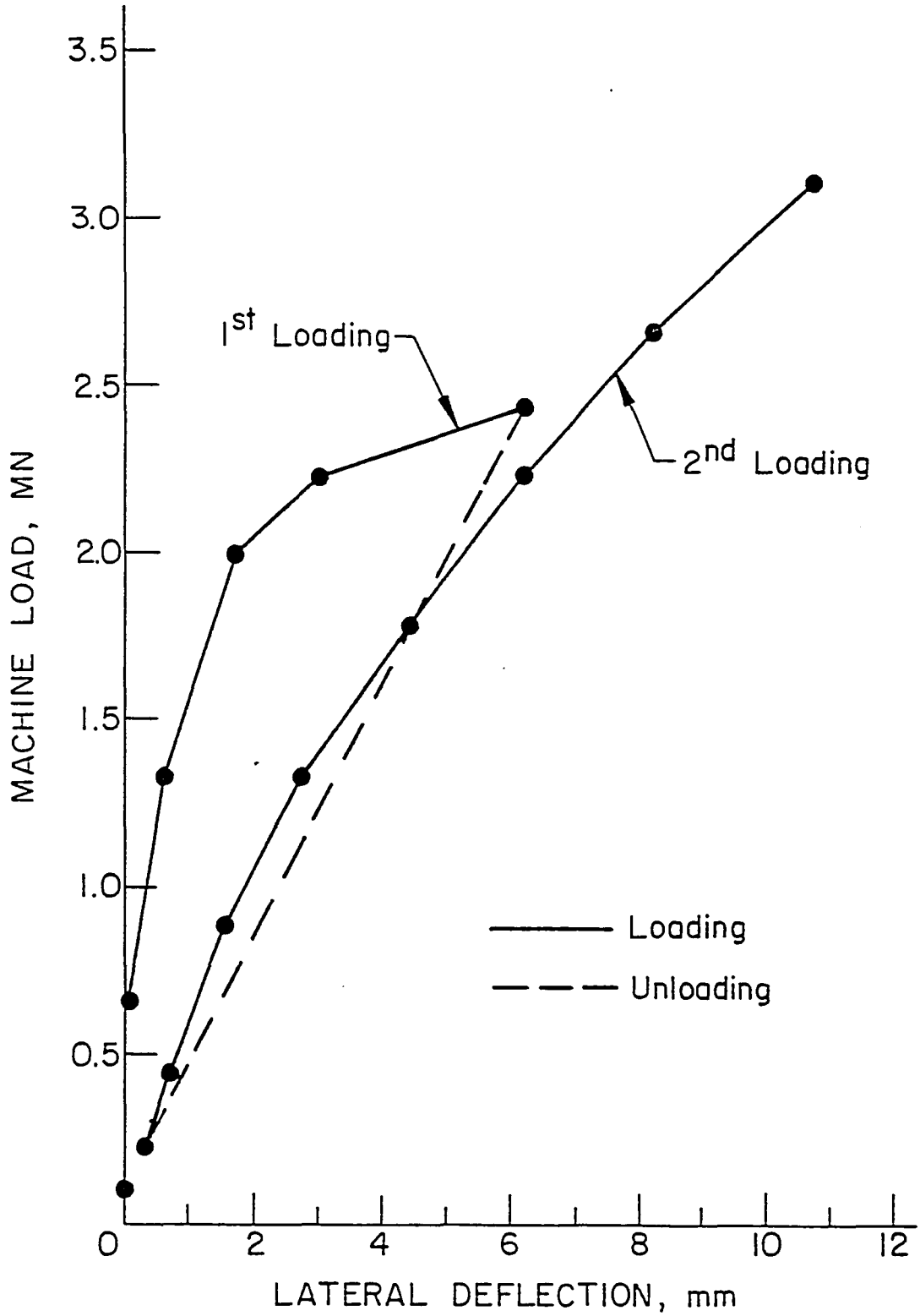

Fig. 29 Critical Sub-Panel Region Grid Point (9, 10)

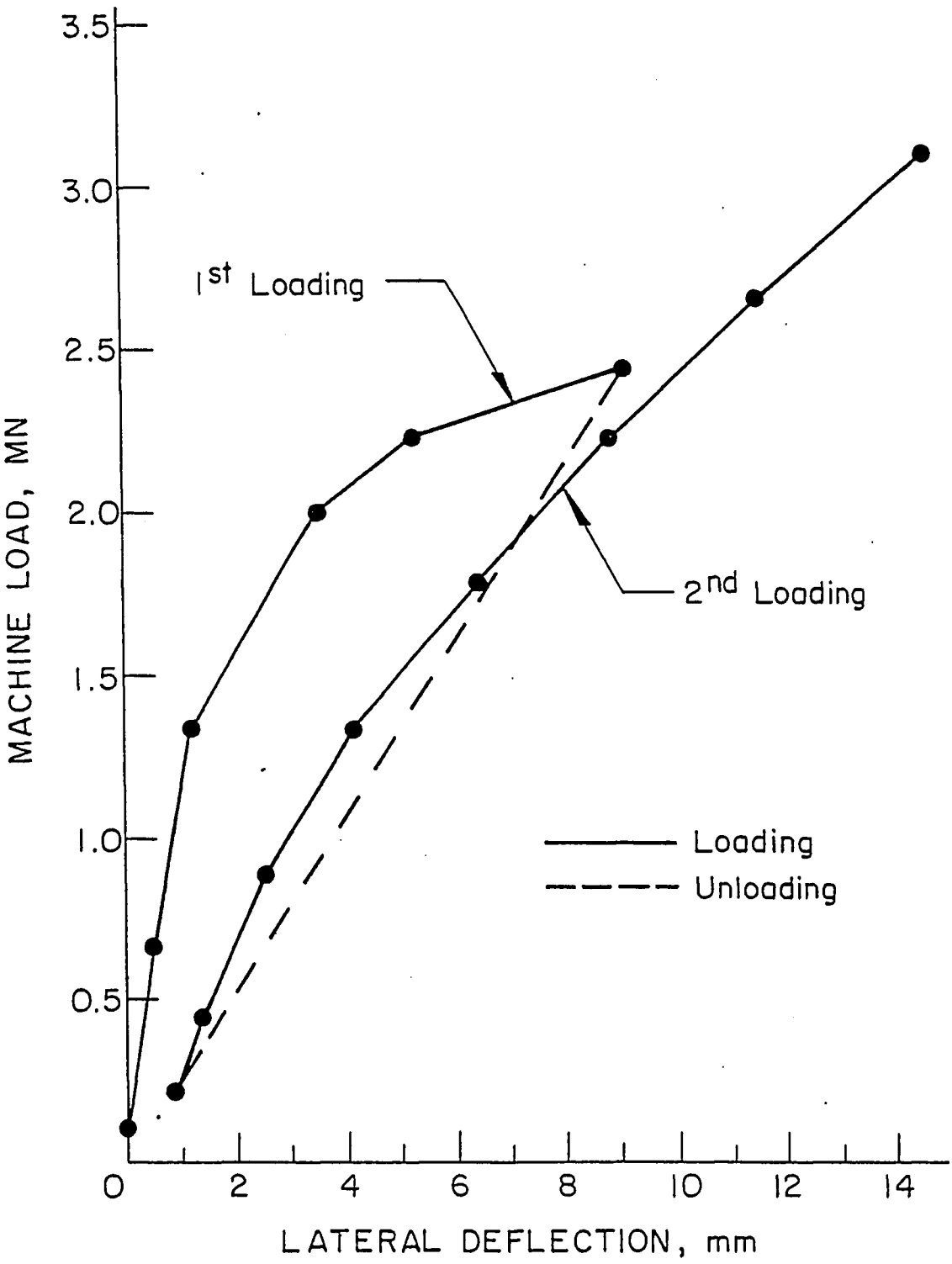

Fig. 30 Critical Sub-Panel Region Grid Point (9, 11)

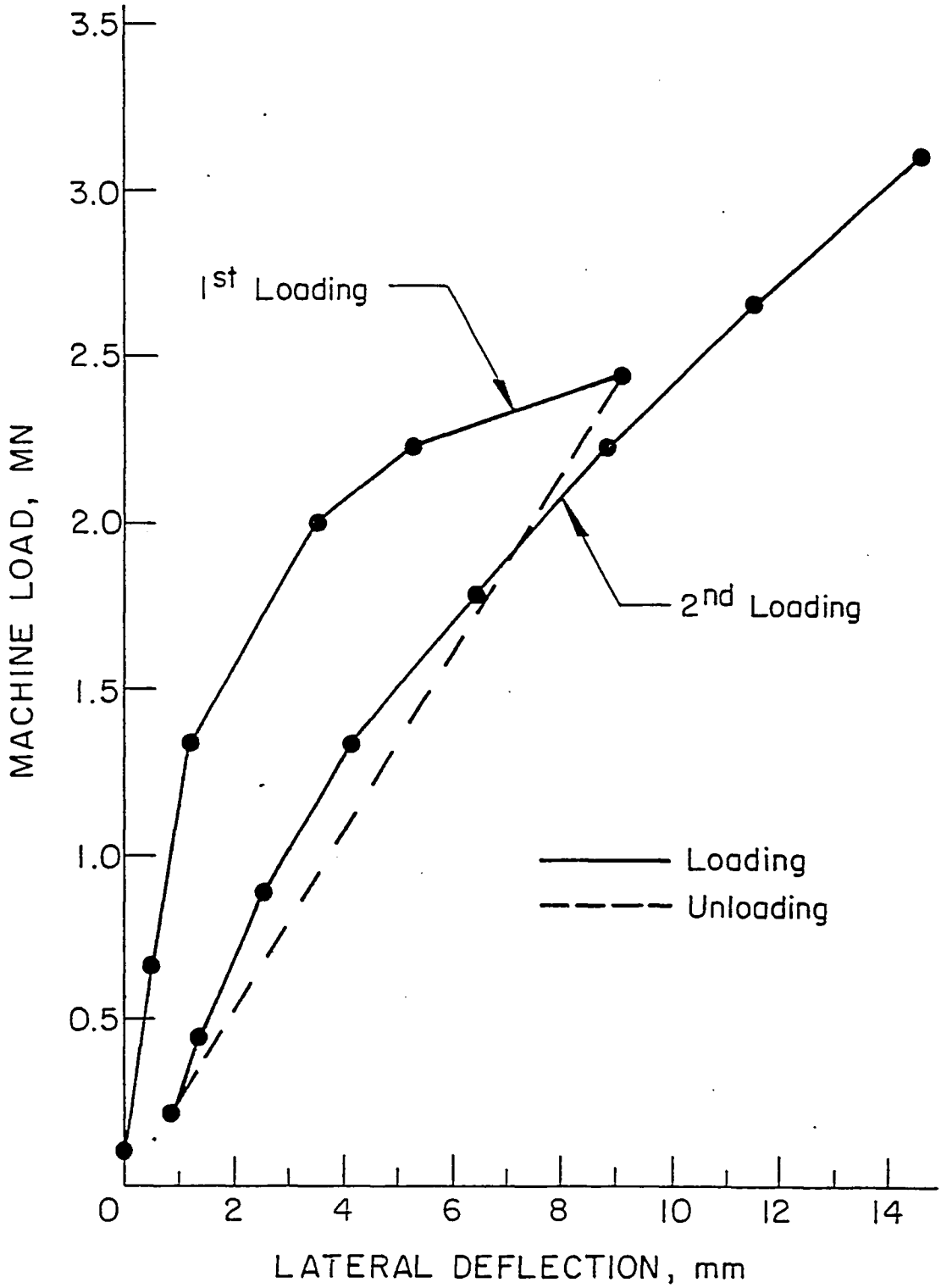

Fig. 30 Critical Sub-Panel Region Grid Point (9, 11)

REFERENCES

1. Richard, R. M. and Troy, R. G.
   STEEL PLATE SHEAR WALLS RESIST LATERAL LOAD, CUT COSTS, ASCE, Vol. 49, No. 3, pp. 53-55, February 1979.

2. Becker, W. F.
   CALIFORNIA HOSPITAL IS QUAKE-PROOF, HIGH-RISE, Engineering News Record, Vol. 201, No. 6, pp. 20-21, August 10, 1978.

3. Lev Zetlin Associates, Inc.
   DESIGN PROCEDURE FOR EXTERIOR PANELS, unpublished design outline, New York, New York, 1981.

4. Lev Zetlin Associates, Inc.
   STRUCTURAL LOAD TEST PROGRAM FOR STEEL FACADE PANEL, unpublished test program, New York, New York, 1981.

5. Slutter, R. G.
   LOAD TEST OF STEEL FACADE PANEL FOR DRAVO BUILDING, unpublished preliminary test report, Fritz Engineering Laboratory, Lehigh University, Bethlehem, PA., 1981.

6. Tall, et al
   STRUCTURAL STEEL DESIGN, Ronald Press, New York, New York, 1974.

7. American Iron and Steel Institute
   COLD-FORMED STEEL DESIGN MANUAL, AISI, Washington, D. C., 1977.

8. Ostapenko, Alexis
   PLATE AND SHELL THEORY, unpublished CE 454 class notes, Lehigh University, Bethlehem, PA. 1982.

9. Schleicher, F.
   TASCHENBUCH FÜR BAUINGENIEURE, Springer-Verlag, 1949.

10. Bendigo, R. A., Hansen, R. M. and Rumpf, J. L.
    LONG BOLTED JOINTS, Journal of the Structural Division, ASCE, Vol. 89, ST6, December 1963.

11. Shanley, F. R.
STRENGTH OF MATERIALS, McGraw Hill, New York, New York, 1957.

12. Batdorf, S. B. and Stein, Manual
CRITICAL COMBINATIONS OF SHEAR AND DIRECT STRESS FOR SIMPLY SUPPORTED RECTANGULAR FLAT PLATES, N.A.C.A. Technical Note No. 1223, Washington, D. C., March 1947.

13. Tide, Raymond H. R.
ECCENTRICALLY LOADED WELD GROUPS - AISC DESIGN TABLES, AISC Engineering Journal, Fourth Quarter, 1980.

14. Butler, L. J. and Kulak, G. L.
STRENGTH OF FILLET WELDS AS A FUNCTION OF DIRECTION OF LOAD, Welding Journal, Welding Research Council, Vol. 36, No. 5, pp. 231-234, May 1971.

15. Fisher, J. W. and Struik, J. H. A.
GUIDE TO DESIGN CRITERIA FOR BOLTED AND RIVETED JOINTS, John Wiley & Sons, New York, New York, 1974.

16. Galambos, T. V.
STRUCTURAL MEMBERS AND FRAMES, St. Louis, MO., 1978.

NOMENCLATURE

A	stiffener area
a	longitudinal plate length
b	effective design width or transverse plate length
b_e	effective width
c	stiffener spacing
E	Young's modulus of elasticity
f	actual stress in a compression element computed on the basis of the effective design width
h	plate thickness
I_r	moment of inertia of a stiffener
i	integer counter
K_s	buckling coefficient
L	member length
N_{xy}	uniform shear load
r	$\sqrt{I/A}$
S	distance from plate centroid to stiffener centroid
t	plate thickness
w/t	flat-width-to-thickness ratio
x	distance in the direction of the member's length
α	aspect ratio, a/b
α_i	$(\pi/L)_i$
γ	shear strain

ν	Poisson's ratio
σ_{cr}	critical normal stress
σ_p	maximum principal stress; (+) means tensile stress; (-) means compressive stress
σ_q	minimum principal stress
σ_x	normal transverse stress in the x-direction
σ_y	normal longitudinal stress in the y-direction
τ_{xy}	shearing stress in the x-y plane
$\tau_{xy_{cr}}$	critical shear stress
ϕ	stress function
ϕ_p	angle from x-axis to σ_p; (+) means counter-clockwise
∇^2	Laplace operator; $\nabla^2 = \frac{\partial^2}{\partial x^2} + \frac{\partial^2}{\partial y^2}$
∇^4	$\nabla^2 \nabla^2$

APPENDICES

APPENDIX A Principal and Orthogonal Stresses

APPENDIX B In-Plane Deformations

APPENDIX C Window Diagonal Deformations

APPENDIX D Conversion Factors

APPENDIX A

TABLE 1 TEST RESULTS: GAGES 1-3

Day	Load (kN)	σ_p (MPa)	σ_q (MPa)	ϕ_p (degrees)	σ_x (MPa)	σ_y (MPa)	τ_{xy} (MPa)
1	445	8.6	- 16.8	40.7	- 2.2	6.1	12.6
	890	19.6	- 37.6	41.7	- 5.8	- 12.3	28.4
	1335	35.4	- 54.6	42.4	- 5.5	- 13.7	44.9
	1780	83.5	- 0.7	63.2	16.4	66.4	33.9
	2225	79.4	- 60.1	47.7	2.9	16.0	69.0
2	445	30.8	- 3.9	69.9	0.2	26.8	11.2
	890	39.5	- 18.8	56.0	- 0.6	21.3	27.0
	1335	50.4	- 35.4	51.1	- 1.5	16.6	42.0
	1780	63.5	- 52.9	48.5	- 1.7	12.4	57.8
	2225	78.0	- 71.1	47.0	- 1.8	8.3	74.5
	2670	95.2	- 86.3	46.5	- 0.3	9.2	91.1
	3115	117.3	- 117.3	43.8	5.2	- 4.6	117.3

TABLE 2 TEST RESULTS: GAGES 4-6

Day	Load (kN)	σ_p (MPa)	σ_q (MPa)	ϕ_p (degrees)	σ_x (MPa)	σ_y (MPa)	τ_{xy} (MPa)
1	445	6.0	- 17.0	32.5	- 0.6	- 10.4	10.4
	890	12.9	- 35.7	31.0	0.0	- 22.8	21.4
	1335	22.8	- 55.3	31.4	1.6	- 34.1	34.7
	1780	29.2	- 73.8	29.3	6.4	- 49.4	44.1
	2225	53.5	- 105.6	32.2	8.3	- 60.4	71.8
2	445	11.1	- 16.1	32.4	3.3	- 8.3	12.4
	890	19.0	- 37.7	31.4	3.7	- 22.3	25.3
	1335	27.5	- 57.7	31.0	5.0	- 35.1	37.6
	1780	36.6	- 78.0	30.7	6.7	- 48.1	50.3
	2225	46.6	- 98.0	30.5	9.5	- 60.7	63.1
	2670	58.1	- 115.9	30.4	13.6	- 71.1	75.9
	3115	74.5	- 125.6	30.9	21.9	- 72.5	88.3

TABLE 3 TEST RESULTS: GAGES 7-9

Day	Load (kN)	σ_p (MPa)	σ_q (MPa)	ϕ_p (degrees)	σ_x (MPa)	σ_y (MPa)	τ_{xy} (MPa)
1	445	0.9	- 29.3	20.4	- 2.7	- 25.7	9.9
	890	2.7	- 61.3	20.0	- 4.8	- 53.8	20.6
	1335	-124.2	- 641.7	61.9	-527.2	- 238.7	214.6
	1780	3.9	- 134.6	21.5	- 14.7	- 115.9	47.3
	2225	10.8	- 168.4	21.7	- 13.7	- 143.5	61.5
2	445	1.1	- 28.0	29.7	- 6.1	- 20.8	12.5
	890	4.0	- 62.9	23.5	- 6.6	- 52.3	24.4
	1335	5.4	- 98.0	22.7	- 10.1	- 82.8	36.8
	1780	6.8	- 133.9	22.5	- 13.7	- 113.2	49.7
	2225	5.0	- 173.9	23.4	- 23.2	- 145.6	65.2
	2670	11.0	- 202.9	23.2	- 22.1	- 169.7	77.3
	3115	21.9	- 238.1	26.0	- 27.9	- 188.4	102.1

TABLE 4 TEST RESULTS: GAGES 10-12

Day	Load (kN)	σ_p (MPa)	σ_q (MPa)	ϕ_p (degrees)	σ_x (MPa)	σ_y (MPa)	τ_{xy} (MPa)
1	445	2.8	- 15.5	36.1	- 3.6	- 9.2	8.7
	890	7.3	- 31.9	36.4	- 6.5	- 18.1	18.7
	1335	15.2	- 43.1	36.9	- 5.8	- 22.0	28.0
	1790	24.4	- 49.8	37.5	- 3.2	- 23.3	35.8
	2225	39.6	- 43.4	37.4	9.0	- 12.8	40.0
2	445	3.0	- 8.3	61.2	- 5.7	0.4	4.8
	890	8.5	- 21.5	44.1	- 6.0	- 7.0	15.0
	1335	16.0	- 32.6	40.7	- 4.6	- 11.9	24.0
	1780	26.6	- 38.7	38.9	0.9	- 13.0	31.9
	2225	40.8	- 37.0	37.3	12.2	- 8.3	37.5
	2670	59.6	- 25.0	36.3	29.9	4.6	40.4
	3115	51.4	- 25.7	35.0	26.0	- 0.3	36.2

TABLE 5 TEST RESULTS: GAGES 13-15

Day	Load (kN)	σ_p (MPa)	σ_q (MPa)	ϕ_p (degrees)	σ_x (MPa)	σ_y (MPa)	τ_{xy} (MPa)
1	445	29.3	0.6	16.6	27.0	2.9	7.9
	890	67.7	- 0.3	17.9	61.3	6.2	19.9
	1335	107.0	0.1	18.5	95.9	10.8	32.2
	1780	135.2	- 1.1	18.2	122.1	12.1	40.4
	2225	157.3	3.1	17.0	144.2	16.2	43.1
2	445	2.5	- 7.0	- 23.2	1.0	- 5.5	- 3.4
	890	36.7	- 2.7	10.5	35.4	- 1.4	7.1
	1335	73.1	- 1.2	14.4	68.7	3.4	18.0
	1780	111.1	0.1	16.1	102.8	8.6	29.6
	2225	148.4	2.3	16.9	135.9	14.6	40.6
	2670	173.9	4.0	16.7	160.0	18.0	46.8
	3115	128.3	31.7	17.0	120.0	40.0	27.0

TABLE 6 TEST RESULTS: GAGES 16-18

Day	Load (kN)	σ_p (MPa)	σ_q (MPa)	ϕ_p (degrees)	σ_x (MPa)	σ_y (MPa)	τ_{xy} (MPa)
1	445	4.4	- 18.6	31.0	- 1.7	- 12.5	10.2
	890	10.2	- 41.0	30.7	- 3.1	- 27.7	22.4
	1335	17.9	- 63.1	30.7	- 3.3	- 42.0	35.6
	1780	26.6	- 85.6	30.8	- 2.8	- 56.1	49.3
	2225	37.0	- 104.9	31.0	- 0.7	- 67.3	62.7
2	445	10.6	- 14.5	34.4	2.6	- 6.5	11.7
	890	16.6	- 38.2	32.0	1.2	- 22.8	24.6
	1335	23.1	- 60.4	31.4	0.5	- 37.7	37.1
	1780	29.9	- 83.5	31.1	- 0.2	- 53.1	50.0
	2225	37.5	- 105.6	31.0	- 0.4	- 67.6	63.1
	2670	46.5	- 124.9	31.1	0.7	- 79.4	75.9
	3115	57.5	- 141.5	34.3	- 5.8	- 78.7	92.5

TABLE 7 TEST RESULTS: GAGES 19-21

Day	Load (kN)	σ_p (MPa)	σ_q (MPa)	ϕ_p (degrees)	σ_x (MPa)	σ_y (MPa)	τ_{xy} (MPa)
1	445	- 0.8	- 3.9	22.5	- 1.2	- 3.5	1.1
	890	- 2.2	- 9.3	28.0	- 3.8	- 7.7	2.9
	1335	- 3.0	- 13.9	29.7	- 5.6	- 11.2	4.7
	1780	- 3.4	- 17.3	31.4	- 7.2	- 13.5	6.2
	2225	- 5.2	- 20.6	35.0	- 10.2	- 15.5	7.2
2	445	0.2	- 8.1	66.0	- 6.8	- 1.2	3.1
	890	- 2.1	- 11.8	55.1	- 8.6	- 5.3	4.5
	1335	- 3.4	- 15.5	48.0	- 10.1	- 8.8	6.1
	1780	- 5.0	- 18.9	42.7	- 11.4	- 12.6	6.9
	2225	- 5.6	- 23.1	41.7	- 13.2	- 15.5	8.7
	2670	- 6.0	- 26.2	43.0	- 15.4	- 16.8	10.1
	3115	- 2.1	- 20.6	53.8	- 14.1	- 8.6	8.8

TABLE 8 TEST RESULTS: GAGES 22-24

Day	Load (kN)	σ_p (MPa)	σ_q (MPa)	ϕ_p (degrees)	σ_x (MPa)	σ_y (MPa)	τ_{xy} (MPa)
1	445	8.1	- 7.7	51.1	- 1.5	1.8	7.7
	890	18.4	- 16.9	50.6	- 2.7	4.2	17.3
	1335	30.2	- 26.0	50.6	- 3.3	7.5	27.5
	1780	43.1	- 34.3	49.6	- 1.8	10.6	38.2
	2225	56.1	- 42.8	49.1	- 0.4	13.7	49.0
2	445	12.3	- 9.0	29.5	7.1	- 3.9	9.2
	890	21.9	- 16.9	40.6	5.5	- 0.4	19.2
	1335	32.8	- 25.4	44.3	4.4	3.0	29.0
	1780	44.6	- 32.8	46.5	3.8	8.0	38.7
	2225	57.6	- 40.8	47.9	3.4	13.5	49.0
	2670	71.1	- 48.2	48.3	4.7	18.4	59.4
	3115	95.2	- 48.7	47.5	17.0	29.7	71.8

TABLE 9 TEST RESULTS: GAGES 25-27

Day	Load (kN)	σ_p (MPa)	σ_q (MPa)	ϕ_p (degrees)	σ_x (MPa)	σ_y (MPa)	τ_{xy} (MPa)
1	445	2.4	- 28.5	31.8	- 6.2	- 19.9	13.9
	890	7.0	- 63.1	30.9	- 11.5	- 44.6	30.9
	1335	12.1	- 97.3	30.9	- 16.8	- 68.4	48.2
	1780	17.2	- 131.8	31.0	- 22.3	- 92.5	65.7
	2225	23.2	- 162.8	31.6	- 27.7	- 111.8	82.8
2	445	8.4	- 21.7	30.3	0.8	- 14.1	13.1
	890	12.4	- 58.0	31.0	- 6.2	- 39.3	31.1
	1335	15.9	- 92.5	31.3	- 13.5	- 63.4	48.2
	1780	19.5	- 129.0	31.5	- 21.1	- 88.3	66.1
	2225	22.4	- 164.9	31.8	- 29.7	- 113.2	84.2
	2670	26.5	- 196.7	32.2	- 36.8	- 133.9	100.7
	3115	46.8	- 188.4	31.0	- 15.5	- 126.3	103.5

TABLE 10 TEST RESULTS: GAGES 28-30

Day	Load (kN)	σ_p (MPa)	σ_q (MPa)	ϕ_p (degrees)	σ_x (MPa)	σ_y (MPa)	τ_{xy} (MPa)
1	445	- 1.6	- 27.0	73.9	- 25.1	- 3.6	6.8
	890	- 3.5	- 57.4	73.2	- 52.9	- 8.0	15.0
	1335	- 4.3	- 84.2	72.4	- 76.6	- 11.7	23.0
	1780	- 7.2	- 102.8	75.0	- 96.6	- 13.7	23.9
	2225	- 12.4	- 122.1	81.4	- 120.1	- 14.9	16.2
2	445	29.3	- 12.4	21.3	23.8	- 7.0	- 14.1
	890	- 6.1	- 15.7	- 48.8	- 11.6	- 10.3	- 4.8
	1335	- 12.4	- 48.0	83.8	- 47.5	- 12.8	3.8
	1780	- 13.0	- 82.8	82.9	- 81.4	- 14.1	8.6
	2225	- 14.5	- 118.0	85.8	- 117.3	- 15.0	7.6
	2670	- 17.9	- 152.5	- 88.1	- 152.5	- 18.0	- 4.5
	3115	- 21.5	- 203.6	- 80.8	- 198.7	- 26.2	- 28.8

TABLE 11 TEST RESULTS: GAGES 31-33

Day	Load (kN)	σ_p (MPa)	σ_q (MPa)	ϕ_p (degrees)	σ_x (MPa)	σ_y (MPa)	τ_{xy} (MPa)
1	445	- 12.4	- 12.4	62.6	- 17.6	- 13.7	2.7
	890	- 22.8	- 49.9	53.9	- 40.5	- 32.2	12.9
	1335	- 33.1	- 84.9	51.1	- 64.2	- 53.4	25.2
	1780	- 48.2	- 118.7	52.0	- 91.8	- 75.2	34.3
	2225	- 50.6	- 182.2	- 46.6	- 120.1	- 112.5	- 65.7
2	445	- 37.7	- 104.2	46.9	- 73.1	- 68.7	33.1
	890	- 47.5	- 131.1	48.3	- 93.8	- 84.9	41.5
	1335	- 56.7	- 156.6	49.2	- 113.9	- 99.4	49.5
	1780	- 66.2	- 184.2	50.2	- 135.9	- 114.5	58.0
	2225	- 75.9	- 213.2	51.1	- 158.7	- 129.7	66.9
	2670	- 135.9	- 494.0	59.7	- 403.0	- 227.0	155.9

TABLE 12 TEST RESULTS: GAGES 34-36

Day	Load (kN)	σ_p (MPa)	σ_q (MPa)	ϕ_p (degrees)	σ_x (MPa)	σ_y (MPa)	τ_{xy} (MPa)
1	445	11.4	- 16.1	38.3	0.8	- 5.5	13.4
	890	25.3	- 37.1	39.1	0.5	- 12.3	30.6
	1335	38.3	- 58.1	39.6	- 0.9	- 18.9	47.4
	1780	51.7	- 80.0	40.2	- 3.2	- 25.2	65.0
	2225	64.0	- 102.1	40.5	- 5.9	- 32.0	82.1
2	445	12.9	- 24.4	48.1	- 7.7	- 3.8	18.6
	890	26.1	- 44.4	43.4	- 7.2	- 11.1	35.2
	1335	38.8	- 63.3	41.8	- 6.6	- 17.9	50.7
	1780	51.6	- 83.5	40.9	- 6.4	- 25.5	66.9
	2225	63.6	- 105.6	40.6	- 7.9	- 34.1	83.5
	2670	74.5	- 129.7	40.5	- 11.4	- 43.3	100.7
	3115	71.1	- 169.1	40.5	- 30.4	- 68.1	118.7

TABLE 13 TEST RESULTS: GAGES 37-39

Day	Load (kN)	σ_p (MPa)	σ_q (MPa)	ϕ_p (degrees)	σ_x (MPa)	σ_y (MPa)	τ_{xy} (MPa)
1	445	7.4	- 16.6	31.8	0.8	- 9.9	10.8
	890	16.0	- 38.4	32.5	0.2	- 22.7	24.7
	1335	24.8	- 58.8	32.7	0.4	- 34.4	38.0
	1780	30.2	- 82.8	32.0	- 1.5	- 51.1	50.8
	2225	37.9	- 104.9	32.4	- 3.0	- 63.8	64.5
2	445	9.5	- 18.0	34.6	0.6	- 9.2	12.8
	890	17.4	- 40.5	33.0	0.3	- 23.3	26.4
	1335	24.7	- 62.3	32.7	- 0.7	- 36.8	39.5
	1780	31.9	- 84.9	32.6	- 2.0	- 50.7	52.9
	2225	38.5	- 107.6	32.7	- 4.1	- 64.8	66.3
	2670	44.9	- 129.7	33.2	- 7.3	- 77.3	80.0
	3115	- 0.3	- 98.0	22.6	- 14.7	- 83.5	34.6

TABLE 14 TEST RESULTS: GAGES 40-42

Day	Load (kN)	σ_p (MPa)	σ_q (MPa)	ϕ_p (degrees)	σ_x (MPa)	σ_y (MPa)	τ_{xy} (MPa)
1	445	2.6	- 26.9	16.3	0.3	- 24.6	7.9
	890	6.3	- 59.5	16.3	1.1	- 54.3	17.7
	1335	10.0	- 91.8	16.1	2.2	- 83.5	27.0
	1780	15.0	- 122.1	14.9	6.0	- 113.2	34.2
	2225	19.8	- 153.2	15.1	8.1	- 141.5	43.5
2	445	5.1	- 26.7	17.6	2.2	- 23.8	9.2
	890	8.8	- 59.7	16.1	3.5	- 54.4	18.3
	1335	12.6	- 91.1	15.8	4.9	- 83.5	27.3
	1780	16.3	- 122.8	15.6	6.3	- 113.2	36.1
	2225	20.1	- 154.6	15.3	7.9	- 142.8	44.5
	2670	24.5	- 183.5	15.5	9.7	- 168.4	53.4
	3115	34.3	- 215.3	17.2	12.6	- 193.2	70.4

TABLE 15 TEST RESULTS: GAGES 43-45

Day	Load (kN)	σ_p (MPa)	σ_q (MPa)	ϕ_p (degrees)	σ_x (MPa)	σ_y (MPa)	τ_{xy} (MPa)
1	445	19.9	- 14.8	39.0	- 6.1	- 1.1	17.0
	890	44.0	- 35.4	38.9	12.6	- 4.1	38.8
	1335	65.9	- 59.3	39.1	16.0	- 9.5	61.3
	1780	82.1	- 84.2	39.4	15.1	- 17.2	81.4
	2225	91.8	- 119.4	40.0	4.5	- 32.0	103.5
2	445	26.2	- 19.9	46.1	2.2	- 4.0	23.0
	890	46.4	- 40.2	42.1	7.5	- 1.3	43.1
	1335	64.2	- 62.2	40.8	10.4	- 8.3	62.5
	1780	79.4	- 89.7	40.3	8.8	- 19.1	83.5
	2225	89.0	- 121.4	40.3	0.7	- 33.5	104.2
	2670	91.1	- 158.7	40.8	- 15.6	- 52.1	123.5
	3115	100.1	- 168.4	42.2	- 21.1	- 47.5	133.2

TABLE 16 TEST RESULTS: GAGES 46-48

Day	Load (kN)	σ_p (MPa)	σ_q (MPa)	ϕ_p (degrees)	σ_x (MPa)	σ_y (MPa)	τ_{xy} (MPa)
1	445	21.1	- 1.2	16.7	19.3	0.6	6.1
	890	48.9	- 3.4	17.0	44.4	1.1	14.6
	1335	75.2	- 5.8	18.1	67.5	2.0	23.9
	1780	81.4	- 2.0	2.7	81.4	- 1.9	3.9
	2225	119.4	- 27.7	- 25.7	91.8	0.0	- 57.5
2	445	38.2	- 41.1	- 47.4	- 4.8	1.9	- 39.5
	890	43.5	- 21.9	- 37.6	19.2	2.4	- 31.6
	1335	53.9	- 9.5	- 25.6	42.1	2.3	- 24.7
	1780	70.4	- 3.5	- 15.4	64.9	1.7	- 18.8
	2225	87.6	- 2.7	- 9.4	84.9	- 0.3	- 14.6
	2670	102.1	- 5.1	- 11.0	98.0	- 1.2	- 20.1
	3115	58.0	11.5	14.5	55.1	14.4	11.2

TABLE 17 TEST RESULTS: GAGES 49-51

Day	Load (kN)	σ_p (MPa)	σ_q (MPa)	ϕ_p (degrees)	σ_x (MPa)	σ_y (MPa)	τ_{xy} (MPa)
1	445	6.4	- 18.5	30.7	- 0.1	- 12.0	10.9
	890	15.2	- 41.3	30.1	1.0	- 27.0	24.5
	1335	24.2	- 63.8	30.4	1.7	- 41.3	38.4
	1780	33.1	- 87.6	30.7	1.5	- 56.2	53.1
	2225	41.7	- 109.0	31.4	0.8	- 67.9	66.9
2	445	9.0	- 21.2	40.3	- 3.6	- 8.6	14.9
	890	17.1	- 44.4	34.8	- 2.9	- 24.3	28.8
	1335	25.0	- 66.4	33.2	- 2.4	- 39.0	41.9
	1780	33.4	- 88.3	32.4	- 1.5	- 53.5	55.1
	2225	41.5	- 111.1	32.1	- 1.6	- 68,2	68.8
	2670	49.6	- 131.8	32.7	- 3.4	- 78.7	82.8
	3115	71.8	- 131.1	38.1	- 5.6	- 53.8	98.7

TABLE 18 TEST RESULTS: GAGES 52-54

Day	Load (kN)	σ_p (MPa)	σ_q (MPa)	ϕ_p (degrees)	σ_x (MPa)	σ_y (MPa)	τ_{xy} (MPa)
1	445	10.0	- 0.5	62.6	1.7	7.7	4.3
	890	24.5	0.6	63.7	5.3	19.8	9.5
	1335	39.6	0.0	64.7	7.2	32.4	15.3
	1780	56.4	- 1.2	65.0	9.1	46.2	22.1
	2225	73.1	- 1.0	65.6	11.7	60.2	27.8
2	445	20.0	- 0.2	59.4	5.1	14.8	8.8
	890	33.3	- 0.5	61.4	7.2	25.6	14.3
	1335	46.4	- 1.1	62.7	8.8	36.4	19.3
	1780	60.2	- 1.6	63.9	10.4	48.2	24.4
	2225	74.5	- 2.2	65.1	11.5	61.0	29.4
	2670	89.7	- 3.9	65.4	12.3	73.1	35.3
	3115	97.3	- 41.7	58.3	- 3.3	58.7	62.0

TABLE 19 TEST RESULTS: GAGES 55-57

Day	Load (kN)	σ_p (MPa)	σ_q (MPa)	ϕ_p (degrees)	σ_x (MPa)	σ_y (MPa)	τ_{xy} (MPa)
1	445	23.1	- 26.1	- 43.1	0.1	- 3.1	- 24.5
	890	56.7	- 60.5	- 43.3	1.5	- 5.3	- 58.5
	1335	59.3	- 65.2	- 43.1	1.2	- 7.1	- 62.1
	1780	67.2	- 73.1	- 42.9	2.2	- 7.8	- 69.7
	2225	86.9	- 91.1	- 43.1	3.5	- 8.3	- 89.0
2	445	37.7	- 35.7	45.2	0.8	1.3	36.7
	890	31.0	- 62.7	39.0	- 0.6	- 25.6	45.7
	1335	37.1	- 38.5	42.6	2.4	- 3.8	37.7
	1780	37.0	- 39.3	41.5	3.4	- 5.8	37.9
	2225	37.0	- 40.2	40.7	4.2	- 7.5	38.2
	2670	37.3	- 39.1	40.3	5.3	- 7.1	37.7
	3115	36.7	- 40.8	40.9	3.5	- 7.7	38.4

TABLE 20 TEST RESULTS: GAGES 58-60

Day	Load (kN)	σ_p (MPa)	σ_q (MPa)	ϕ_p (degrees)	σ_x (MPa)	σ_y (MPa)	τ_{xy} (MPa)
1	445	1.8	- 29.9	35.8	- 9.0	- 19.0	15.0
	890	4.5	- 68.7	35.7	- 20.4	- 43.8	34.6
	1335	7.2	- 107.0	35.3	- 31.1	- 68.9	54.0
	1780	10.9	- 144.9	34.5	- 39.1	- 95.2	72.5
	2225	14.0	- 176.6	34.1	- 45.9	- 117.3	88.3
2	445	4.9	- 26.5	20.9	0.9	- 22.5	10.4
	890	5.8	- 64.9	29.4	- 11.2	- 47.9	30.2
	1335	7.9	- 102.1	31.6	- 22.4	- 71.8	49.1
	1780	10.8	- 140.1	32.8	- 33.5	- 95.9	68.8
	2225	13.5	- 178.7	33.5	- 45.0	- 120.1	88.3
	2670	16.6	- 211.8	33.5	- 53.2	- 142.1	105.6
	3115	5.3	- 245.6	29.2	- 54.3	- 185.6	107.0

TABLE 21 TEST RESULTS: GAGES 61-63

Day	Load (kN)	σ_p (MPa)	σ_q (MPa)	ϕ_p (degrees)	σ_x (MPa)	σ_y (MPa)	τ_{xy} (MPa)
1	445	0.7	- 18.5	80.3	- 17.9	0.2	3.2
	890	2.7	- 36.1	82.3	- 35.4	2.0	5.2
	1335	3.3	- 57.1	82.5	- 56.0	2.2	7.8
	1780	3.2	- 74.5	82.8	- 73.1	2.0	9.7
	2225	5.9	- 91.1	82.8	- 89.4	4.4	12.1
2	445	28.8	- 2.2	- 42.1	14.9	11.7	- 15.5
	890	10.4	- 19.5	- 75.1	- 17.6	8.4	- 7.4
	1335	5.3	- 49.3	89.2	- 49.3	5.3	0.7
	1780	4.1	- 78.7	84.1	- 78.0	3.2	8.4
	2225	2.5	- 122.1	79.9	- 118.7	- 1.4	21.6
	2670	7.5	- 155.9	79.0	- 149.7	1.6	30.5
	3115	16.0	- 185.6	79.5	- 178.7	9.2	36.3

TABLE 22 TEST RESULTS: GAGES 64-66

Day	Load (kN)	σ_p (MPa)	σ_q (MPa)	ϕ_p (degrees)	σ_x (MPa)	σ_y (MPa)	τ_{xy} (MPa)
1	445	31.9	- 14.8	- 5.3	31.5	- 14.4	- 4.3
	890	31.1	- 33.4	8.3	29.7	- 32.1	9.2
	1335	29.3	- 61.5	18.6	20.1	- 52.4	27.5
	1780	29.7	- 98.0	23.7	9.0	- 77.3	47.1
	2225	109.0	- 89.7	12.9	99.4	- 79.4	43.3
2	445	- 5.7	- 24.4	24.2	- 8.9	- 21.3	7.0
	890	- 12.8	- 50.7	33.0	- 24.1	- 39.5	17.3
	1335	- 17.9	- 74.5	35.6	- 37.1	- 55.4	26.8
	1780	- 22.8	- 98.7	37.4	- 50.8	- 70.4	36.7
	2225	- 23.0	-116.6	36.7	- 56.5	- 83.5	45.0
	2670	- 6.1	-153.9	33.4	- 50.8	- 109.0	67.9
	3115	56.3	-182.9	27.7	4.5	- 131.1	98.7

APPENDIX B IN-PLANE DEFORMATIONS

Load (kN)	1 (mm)	2 (mm)	3 (mm)	4 (mm)	5 (mm)	6 (mm)	7 (mm)	8 (mm)	9 (mm)
107	0.00	0.00	0.00	0.00	0.00	0.00	0.00	0.00	0.00
223	1.55	0.10	0.81	0.33	0.25	0.33	0.25	0.53	0.51
445	2.77	0.03	2.18	0.94	0.51	0.61	0.76	0.46	-1.02
668	3.66	0.10	3.10	1.12	0.76	1.17	1.02	0.53	-1.52
890	4.47	0.28	4.09	1.30	1.02	0.97	1.52	0.38	-1.78
1113	5.16	0.43	5.05	1.42	1.27	1.32	1.78	0.58	-2.29
1335	5.74	0.58	5.99	1.60	1.27	2.08	2.29	0.71	-2.79
1558	6.43	0.74	7.24	2.11	1.52	1.70	2.54	0.97	-3.30
1780	7.16	0.91	8.00	2.34	1.78	1.93	3.05	1.04	-3.81
2003	7.87	1.12	9.04	2.41	2.03	1.93	3.30	1.22	-4.06
2225	8.38	1.30	10.01	2.72	2.29	1.98	3.81	1.40	-4.57
2448	9.53	1.52	11.46	2.79	2.54	2.01	4.06	1.57	-5.08
2670	9.78	1.65	12.27	3.25	--	2.39	--	1.80	--
3115	15.88	2.36	15.75	3.73	--	2.72	--	2.39	--

Note: Sign convention: (-) lengthening of given dimension

APPENDIX C WINDOW DIAGONAL DEFORMATION

Day	Load (kN)	1 (mm)	2 (mm)	3 (mm)	4 (mm)	5 (mm)	6 (mm)
1	0	0.000	0.000	0.000	0.000	0.000	0.000
	223	-0.216	0.086	-0.015	0.155	-0.071	0.103
	445	-0.201	0.274	-0.386	0.505	-0.442	0.499
	890	-0.193	0.838	-1.257	1.113	-1.049	1.112
	1113	-0.203	1.120	-1.577	1.420	-1.336	1.413
	1335	-0.221	1.455	-1.961	1.783	-1.676	1.728
	1558	-0.191	1.781	-2.774	2.385	-1.976	2.101
	1780	-0.213	2.294	-3.200	2.565	-2.022	2.412
	2003	-0.142	2.791	-3.701	2.898	-2.677	2.775
	2448	-4.450	3.665	-4.478	3.922	-3.368	3.620
2	223	-1.339	0.688	-1.273	1.641	-0.564	--
	445	-1.514	1.003	-1.638	1.191	-0.833	1.047
	1335	-2.858	2.090	-2.830	2.370	-1.869	2.175
	1780	-3.513	2.690	-3.487	2.962	-2.403	2.764
	2670	-7.252	4.186	-5.080	4.402	-3.724	4.104
	3115	-6.050	6.045	-7.333	6.010	-5.288	5.430

Note: Sign convention: (-) indicates diagonal shortening

APPENDIX D CONVERSION FACTORS

1 inch = 2.54 centimeters = 25.4 millimeters

1 foot = 0.305 meters

1 kip = 4.45 kN

1 ksi = 6.9 MPa

VITA

William DeForrest Bast, son of Joanne S. and DeForrest S. Bast, was born on September 11, 1957 in Fountain Hill, Pennsylvania. The author spent the majority of his childhood and adolescence in Emmaus, Pennsylvania, graduating in 1975 from Emmaus High School.

The author attended Lehigh University in Bethlehem, Pennsylvania and received the Bachelor of Science degree in Civil Engineering in June of 1979. Immediately after graduation he accepted a position as a Manufacturing Manager at the Procter and Gamble Paper Products Company in Mehoopany, Pennsylvania. In 1980 he was promoted to Project Engineer at the same location.

Mr. Bast returned to Lehigh University in July of 1981 as a Research Assistant in the Operations Division of Fritz Engineering Laboratory. He will receive the Master of Science degree in Civil Engineering on June 5, 1983. Mr. Bast has accepted the position of structural engineer with the partnership of Skidmore, Owings and Merrill and plans to commence work in Chicago on July 5, 1983.

TABLE 11 RESULTS VERSUS ANALYSIS - GAGES 31-33 AND 64-66

Day	Load (kN)	RESULTS						ANALYSIS					
		FRONT			BACK			VIERENDEEL TRUSS			PLANE STRESS		
		σ_x (MPa)	σ_y (MPa)	τ_{xy} (MPa)	σ_x (MPa)	σ_y (MPa)	τ_{xy} (MPa)	σ_x (MPa)	σ_y (MPa)	τ_{xy} (MPa)	σ_x (MPa)	σ_y (MPa)	τ_{xy} (MPa)
1	445	- 17.6	- 13.7	2.7	31.5	- 14.4	- 4.3	--	- 15.0	2.1	0.0	0.0	6.1
	890	- 40.5	- 32.2	12.9	29.7	- 32.1	9.2	--	- 30.0	4.2	0.0	0.0	12.2
	1335	- 64.2	- 53.4	25.2	20.1	- 52.4	27.5	--	- 45.0	6.3	0.0	0.0	18.3
	1780	- 91.8	- 75.2	34.3	9.0	- 77.3	47.1	--	- 60.0	8.4	0.0	0.0	24.4
	2225	-120.1	-112.5	- 65.7	99.4	- 79.4	43.3	--	- 75.0	10.5	0.0	0.0	30.5
2	445	- 73.1	- 68.7	33.1	- 8.9	- 21.3	7.0	--	- 15.0	2.1	0.0	0.0	6.1
	890	- 93.8	- 84.9	41.5	- 24.1	- 39.5	17.3	--	- 30.0	4.2	0.0	0.0	12.2
	1335	-113.9	- 99.4	49.5	- 37.1	- 55.4	26.8	--	- 45.0	6.3	0.0	0.0	18.3
	1780	-135.9	-114.5	58.0	- 50.8	- 70.4	36.7	--	- 60.0	8.4	0.0	0.0	24.4
	2225	-158.7	-129.7	66.9	- 56.5	- 83.5	45.0	--	- 75.0	10.5	0.0	0.0	30.5
	2670	-251.2	-164.9	100.1	- 50.8	-109.0	67.9	--	- 90.0	12.6	0.0	0.0	36.6
	3115	-403.0	-227.0	155.9	4.5	-131.1	98.7	--	-105.0	14.6	0.0	0.0	42.7